Michelson

BRL R 1596

BRL

AD

REPORT NO. 1596

ANALOG SIMULATION OF THE MECHANISM OF THE M16A1 RIFLE

by

Herman P. Gay
Emma M. Wineholt

June 1972

U.S. ARMY ABERDEEN RESEARCH AND DEVELOPMENT CENTER
BALLISTIC RESEARCH LABORATORIES
ABERDEEN PROVING GROUND, MARYLAND

When this report is no longer needed, Department of the Army organizations will destroy it in accordance with the procedures given in AR 380-5. Navy and Air Force elements will destroy it in accordance with applicable directives. Department of Defense contractors will destroy the report according to the requirements of Section 14 of the Industrial Security Manual for Safeguarding Classified Information. All others will return the report to Commanding Officer, U.S. Army Aberdeen Research and Development Center, Aberdeen Proving Ground, Maryland.

Secondary distribution of this report by originating or sponsoring activity is prohibited.

Additional copies of this report may be obtained from the Defense Documentation Center, Cameron Station, Alexandria, Virginia 22314

The findings in this report are not to be construed as an official Department of the Army position, unless so designated by other authorized documents.

The use of trade names or manufacturers' names in this report does not constitute indorsement of any commercial product.

B A L L I S T I C R E S E A R C H L A B O R A T O R I E S

REPORT NO. 1596

JUNE 1972

ANALOG SIMULATION OF THE MECHANISM OF THE M16A1 RIFLE

Herman P. Gay
Emma M. Wineholt

Interior Ballistics Laboratory

AMCMS Code No. 4420.16.0132.251

PRON. No. 45-9-76500-(02)-45-AJ

A B E R D E E N P R O V I N G G R O U N D, M A R Y L A N D

B A L L I S T I C R E S E A R C H L A B O R A T O R I E S

REPORT NO. 1596

HPGay/EMWineholt/cs
Aberdeen Proving Ground, Md.
June 1972

ANALOG SIMULATION OF THE MECHANISM OF THE M16A1 RIFLE

ABSTRACT

The mechanism of the M16 Rifle has been simulated in some detail on the analog computer. This simulation yields the linear motion of the gun, the linear and the angular motion of the bolt, the linear motion of the carrier and the angular motion of the hammer. During the course of the work techniques were adapted and extended for calculating linear impulsive motion, a combination of linear and angular impulsive motions and the dynamics of cam systems. As a result, the output of the simulation agrees rather well with the measured motion. However, the more important aspect of this study is that the engineer now has at hand the basic techniques, or tools, for modeling self-powered automatic weapon mechanisms.

TABLE OF CONTENTS

		Page
	ABSTRACT	3
	LIST OF ILLUSTRATIONS	7
	LIST OF SYMBOLS	9
I.	INTRODUCTION	13
II.	MODEL OF THE RIFLE	14
III.	THE CONTACT FORCES	17
IV.	THE FORCES DUE TO PRESSURE	24
	A. The Powder Pressure	24
	B. The Carrier Cavity Pressure	27
	C. The Control Circuit for the Pressures	28
V.	THE BOLT MOTION	29
	A. The Linear Motion	29
	B. The Angular Motion	32
VI.	THE CARRIER MOTION	35
VII.	THE GUN MOTION	39
VIII.	THE HAMMER MOTION	39
IX.	RESULTS	45
X.	RESUME	52
	ACKNOWLEDGMENTS	54
	REFERENCES	55
	DISTRIBUTION LIST	57

LIST OF ILLUSTRATIONS

Figure		Page
1.	Rifle Mounted for Firing.	14
2.	Mechanism of the M16A1 Rifle.	15
3.	Major Components of the Rifle	16
4.	Impact From the Left.	18
5.	Impact From Either Side	18
6.	Impact Force vs Displacement.	19
7.	Bouncing Ball	19
8.	Coefficient of Restitution vs Damping Coefficient	20
9.	Damped Impact Between Two Masses.	21
10.	Analog Diagrams for Two-Body Impact	22
11.	Combined Linear and Angular Impact.	23
12.	Circuits for Generating the Powder Pressure-Time Curve. .	25
13.	Pressure-Time Curves.	26
14.	Circuits for Generating the Pressure in the Carrier Cavity.	27
15.	Control Circuits.	28
16.	Schematic Diagram of Components	29
17.	Circuits for Generating the Locking Force	30
18.	Circuits for Calculating the Linear Motion of the Bolt. .	31
19.	Diagram of Bolt Forces.	32
20.	The Cam Track and Its Derivative.	33
21.	Circuits for Generating F_α and F_z	33
22.	Circuits for Calculating the Angular Displacement of the Bolt.	34

LIST OF ILLUSTRATIONS (Cont'd)

Figure		Page
23.	Circuits for Generating the Limit Stop Forces.	35
24.	Driving Spring Force	36
25.	Circuits for Generating the Driving Spring Force	36
26.	Circuits for Generating F_{12} and F_B	37
27.	Circuits for Calculating the Carrier Motion.	38
28.	Circuits for Calculating the Gun Motion.	38
29.	Carrier-Hammer Diagram	41
30.	Circuits for Generating the Torques on the Hammer. . . .	42
31.	Hammer Rotation vs Carrier Displacement.	43
32.	Circuits for Generating the Hammer-Carrier Force	44
33.	Circuits for Calculating the Angular Displacement of the Hammer.	44
34.	Displacements and Velocities vs Time	45
35.	Forcing Functions.	46
36.	Initial Velocities	47
37.	Hammer Rebound	49
38.	Interaction of Hammer and Carrier.	50
39.	Phase-Plane Diagram of Carrier Motion.	51

LIST OF SYMBOLS

Symbol	Parameter	Dimensions	Value
a	position of limit stop	in.	.30
A_b	cross-sectional area of the bore	$in.^2$	.038
A_1	area of the interior base of cartridge case	$in.^2$	.071
A_{23}	cross-sectional area of the carrier cavity	$in.^2$	.172
b	position of limit stop	in.	.325
d	distance	in.	
D	damping coefficient	lb sec/in.	
D_B	damping coefficient (buffer)	lb sec/in.	1.63
D_{12}	damping coefficient between gun and carrier	lb sec/in.	20.99
D_{13}	damping coefficient between gun and bolt	lb sec/in.	7.49
D_{23}	damping coefficient between carrier and bolt	lb sec/in.	7.12
D_{24}	damping coefficient between carrier and hammer	lb sec/in.	5.40
D_4	damping coefficient between hammer and solid stop	lb in. sec	5.58
F	force	lb	
I	moment of inertia	lb in. sec^2	
I_3	moment of inertia of bolt	lb in. sec^2	1.442×10^{-5}
I_4	moment of inertia of hammer	lb in. sec^2	1.765×10^{-4}
k	spring rate	lb/in.	10^6
K	spring rate	lb/in.	
K_c	driving spring rate (compression)	lb/in.	1.56
K_r	driving spring rate (release)	lb/in.	1.42
K_B	buffer spring rate	lb/in.	5000.

LIST OF SYMBOLS (Cont'd)

Symbol	Parameter	Dimensions	Value
K_1	recoil spring rate	lb/in.	144.2
$\overline{K}$	torsional spring rate	in. lb/rad	2.02
K	spring rate	in. lb/rad	10^6
ℓ	distance from point of impact to center of rotation	in.	
ℓ_h	distance from hammer pivot to carrier	in.	.95
m_1	mass of gun	lb sec^2/in.	.03350
m_2	mass of carrier	lb sec^2/in.	$.2699 \times 10^{-2}$
m_3	mass of bolt	lb sec^2/in.	$.3212 \times 10^{-3}$
M	mass	lb sec^2/in.	
p	carrier cavity pressure	psi	
P	powder pressure	psi	
r_c	centroid of cam surface	in.	.38
r_ℓ	centroid of lugs	in.	.318
R	coefficient of restitution		.5 (mostly)
T	torque	in. lb	
T_g	accelerating torque	in. lb	
T_o	initial torque	in. lb	3.35
W	weight	lb	
x	displacement	in.	
z	relative displacement between carrier and bolt	in.	
α	angular displacement of bolt	rad	
β	time scaling constant		10^{4*}
δ_B	distance	in.	3.80
δ_D	distance	in.	3.48
Δ	clearance	in.	.003
ε	deformation	in.	
ζ	damping coefficient		

*For plotting the complete cycle β was made equal to 10^3 by removing the .1β plugs.

LIST OF SYMBOLS (Cont'd)

Symbol	Parameter	Dimensions	Value
θ	angular displacement of the hammer	rad	
λ	distance from 0 to CG	in.	
μ	coefficient of friction		.25
ϕ	function		
ψ	function		
ω	frequency	rad/sec	

SUBSCRIPTS

a	position of limit stop	R	recoil spring
b	position of limit stop	s	hammer spring
B	buffer	z	relative displacement of carrier and bolt
D	driving spring	α	bolt
h	hammer	θ	hammer
i	any component	1	gun
j	any component	2	carrier
ℓ	hammer latch	3	bolt
m	hammer limit stop	4	hammer
p	cavity pressure		

NOTATION

RC	relay comparator
EC	electronic comparator
SCR	silicon-controlled rectifier
$\dot{x}$	dx/dt
$\ddot{x}$	d^2x/dt^2

I. INTRODUCTION

Extensive use of the new M16 Rifle in Southeast Asia led to allegations that it was not reliable. In November 1967 the Weapons Systems Evaluation Group was given the responsibility for directing a test to measure the operational reliability of the 5.56mm, M16A1 Rifle Systems. The results of those tests[1*] showed that there were a number of malfunctions, some of which could be associated with the kind of propellant used in the ammunition.

The USAMC Project Manager for Rifles organized the M16 Advisory Group to coordinate the effects of all USAMC Agencies participating in the production and the improvement of the rifle and the ammunition. At the first meeting of the Group in February 1968, the Interior Ballistics Laboratory of BRL was assigned the studies of interior ballistics and weapon kinematics. A plan for two and one-half years of effort was presented to the project manager and funds were received in July 1968. It was soon evident that the original scope of work at the IBL was not sufficiently broad. For example, a detailed analysis of the gas-operating system was found to be necessary to establish the interaction between the interior ballistics and the dynamics of the mechanism. In addition, various ad hoc studies such as the effect of cyclic rate on parts breakage and the performance of the mechanism at extreme temperatures were carried out upon the request of the project manager. The results of these ad hoc studies have been given in briefings, progress reports and letter reports. The interior ballistic study is given in reference 2. The analysis of the gas-operating system is given in references 3 and 4. Reference 5 gives the results of experiments to measure the pressures in the gas-operating system and their effect on the gun mechanism.

From the onset it was felt that a physical-mathematical model of the rifle mechanism was essential to the understanding of its operation, or

---

*Superscript numbers indicate references at the end of this report.

performance. This report utilizes most of the techniques that have been developed at the Ballistic Research Laboratories for simulating (or modeling) automatic weapons.[6,7] Some of those techniques were developed under other projects. Most of them have been reported informally at seminars, status meetings and briefings.

To establish a reasonably complete simulation this study consisted of four phases:

1. Measurements of the masses, moments of inertia, spring rates and distances were made to provide basic input data for the model. (Those data are given in the List of Symbols.)

2. Firing tests were conducted to measure pressures in the chamber, at the port, and in the carrier cavity. These pressure-time curves provided the forcing functions for the model. Displacement-time curves of the main components of the mechanism were also recorded.*

3. Mathematical, or physical, models were developed so that the mechanism could be simulated on an analog computer.

4. Comparisons of the simulated, or calculated, displacements and velocities were made with those observed in the firing tests to assess the adequacy of the models.

II. MODEL OF THE RIFLE

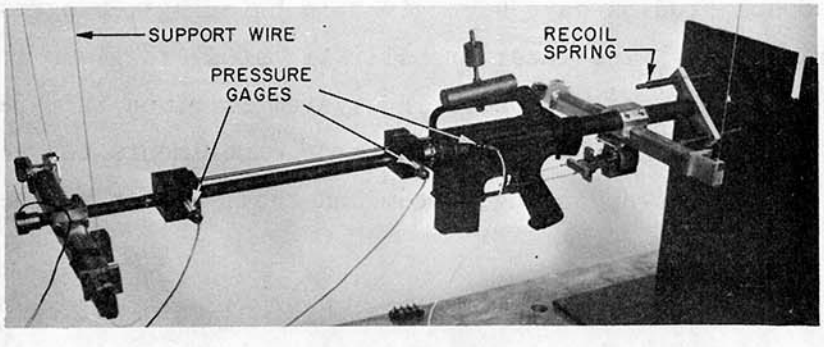

Figure 1. Rifle Mounted for Firing

*See Reference 5

Experience has shown that a rifleman may not be consistent in the way that he holds the rifle and responds to the firing impulse. Thus, to provide consistent, measurable performance of the rifle it was held in the mechanical support shown in Figure 1.

The supporting wires of the ballistic pendulum restrained all motion except recoil. The recoil was restrained by four helical springs, two pairs in parallel, and each pair acting in series. In this way, the recoil force was a consistent, measurable function of the distance, uncomplicated by friction.

No attempt was made to simulate the rifleman because that is a complex problem in itself. However, when the rifleman's body can be characterized (or simulated) by some dynamic system, that system can be substituted for the simple spring-mass system of this study.

The rifle consists of a series of complex, interacting parts that feed the ammunition, fire the projectile, and extract and eject the empty cartridge case. Figure 2 shows the mechanism.

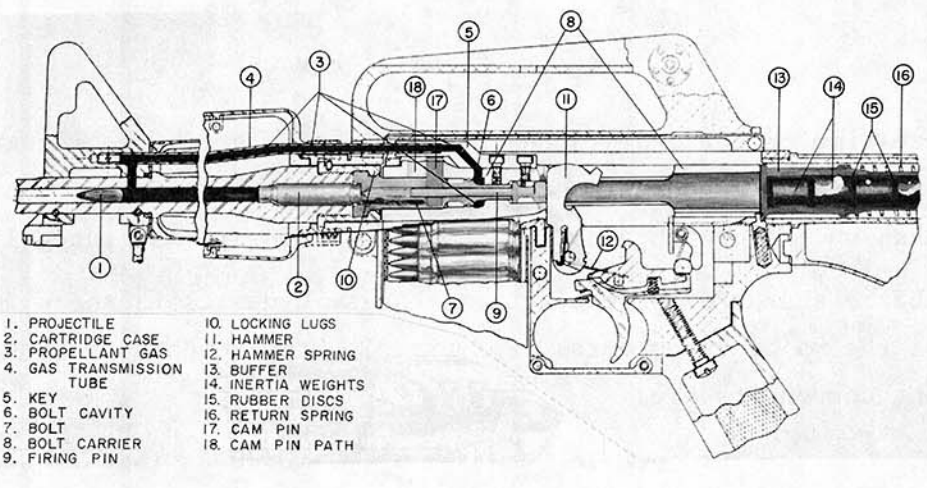

Figure 2. Mechanism of the M16A1 Rifle

A complete description of the mechanism and its operation is given in the Technical Manual.[8]

The rifle can be divided into four major components to describe

the dynamic behavior. Figure 3 shows those components.

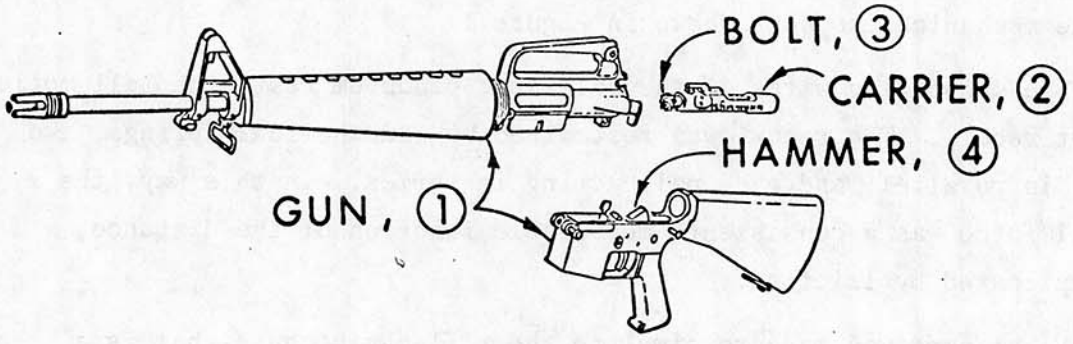

Figure 3. Major Components of the Rifle

The circled numbers after each component are used as subscripts to denote the mass or displacement of that particular component; e.g., m_3 is the mass of the bolt.

The system is simulated by generating the forces that act on each mass. The equation of motion of any component, i, is then written simply as:

$$m_i \ddot{x}_i = \text{Sum of Forces.}$$

The force-time or force-distance curves are simulated (or generated) by the electrical components of the analog computer. The motion of the mechanism is then obtained by summing the forces and integrating.

A basic characteristic of gun mechanism dynamics is the wide range of the major parameters. For example, the weights of some important components are:

Projectile	0.00786 lbs.
Bolt	0.1235 lbs.
Carrier	1.042 lbs.
Gun	12.93 lbs.

The range is thus about 1 to 1500. Now, there is a corresponding range of forces and their duration as indicated below:

Event	Duration, millisec.
Metal-on-metal impact	0.1 or less
Powder pressure	1
Bolt locking and unlocking	2-3
Carrier motion (cycle time)	100

The range of the various parameters turns out to be quite natural when one considers that the basic problem is to transmit the momentum of the projectile and powder gases to the ground. The initial, large, powder-pressure force is transmitted to successively larger masses, with consequently smaller velocities and longer times. Thus, when the momentum is imparted to the rifleman's shoulder, the associated force is acceptably small because it lasts for a relatively long time.

The wide range of the parameters implies that the computer resolution in force (voltage in the computer) and time must be better than 1:1000. Stated another way -- the analog computer circuits must have good response up to high frequency and must have small, long-term drift. By proper attention to detail and the scaling of the various parameters a satisfactory solution can be obtained.

III. THE CONTACT FORCES

In this rifle the contact forces (i.e., impact and locking forces) are very important because every component makes metal-on-metal contact with another component at some time during the cycle. A technique developed by J. P. Laird[9] has been adapted to this problem; and, since it will be used over and over again, some general procedures will be developed here.

Consider the two impacting masses shown in Figure 4.

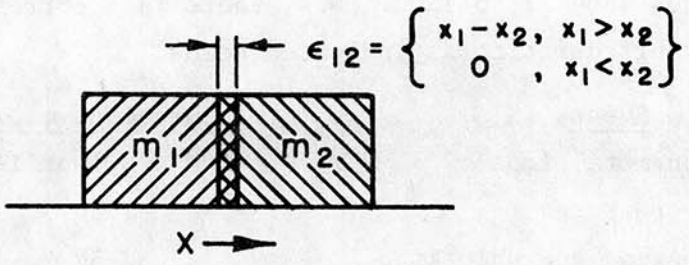

Figure 4. Impact From the Left

When m_1 strikes m_2 a force F_{12} will be developed, and

$$m_1 \ddot{x}_1 = -F_{12}$$

$$m_2 \ddot{x}_2 = +F_{12}, \text{ where}$$

$$F_{12} = +k\varepsilon_{12}, \text{ where}$$

k = a very large spring rate

ε = the "deformation"

$$\varepsilon_{12} = \begin{cases} x_1 - x_2, & (x_1 - x_2) \geq 0 \\ 0, & (x_1 - x_2) < 0 \end{cases}.$$

There will be some instances where m_1 strikes m_2 from either direction as shown in Figure 5.

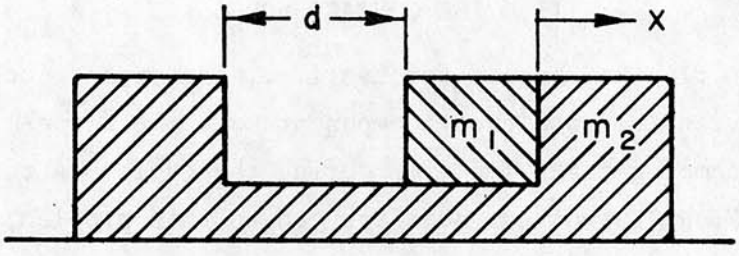

Figure 5. Impact From Either Side

In the above Figure, F_{12} is as described previously. However,

$$F_{21} = +k\varepsilon_{21}$$

$$\varepsilon_{21} = \begin{cases} (x_2 - x_1) - d, & (x_2 - x_1) - d \geq 0 \\ 0, & (x_2 - x_1) - d < 0 \end{cases}.$$

The forces are illustrated in Figure 6.

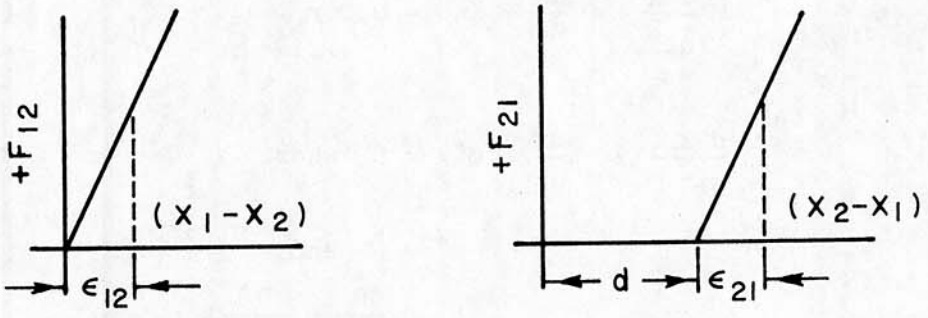

Figure 6. Impact Force vs Displacement

In the analog computer, the contact force is generated by a high-gain, half-wave rectifier. For extremely high impact forces, additional gain can be attained by entering the integrator with a gain of ten or more. This generally will not overload the integrator because the impact forces last only a short time.

Actual impacts generally are not elastic. Laird's illustration of a bouncing ball with damping is shown in Figure 7.

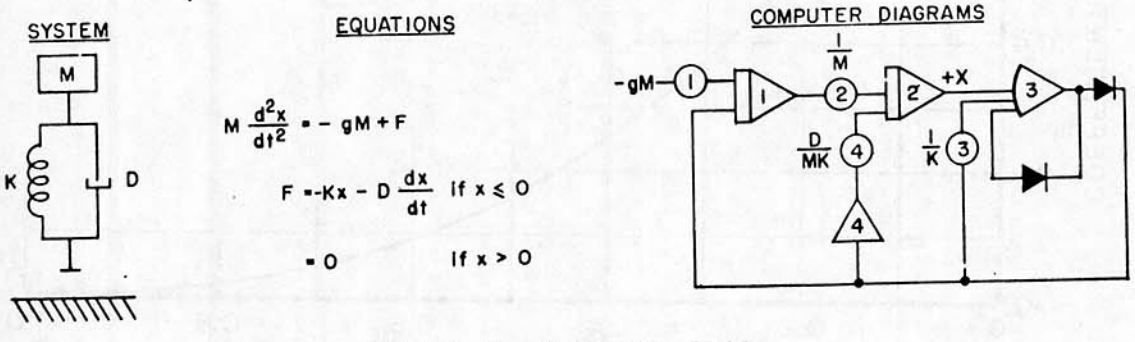

Figure 7. Bouncing Ball

In engineering practice damped impact is usually represented by a coefficient of restitution, R.

$$R = - \frac{\text{relative velocity of separation}}{\text{relative velocity of approach}} .$$

Consider the usual differential equation:

$$M \frac{d^2x}{dt^2} + D \frac{dx}{dt} + Kx = 0, \text{ or} \qquad (1)$$

$$\frac{d^2x}{dt^2} + 2\zeta \omega \frac{dx}{dt} + \omega^2 x = 0, \text{ where} \qquad (2)$$

$$\omega^2 = \frac{K}{M}, \text{ and}$$

$$\zeta = \frac{D}{2M\omega} = \frac{D}{2\sqrt{KM}} .$$

The relation between ζ and R for the bouncing ball is shown in Figure 8.[9]

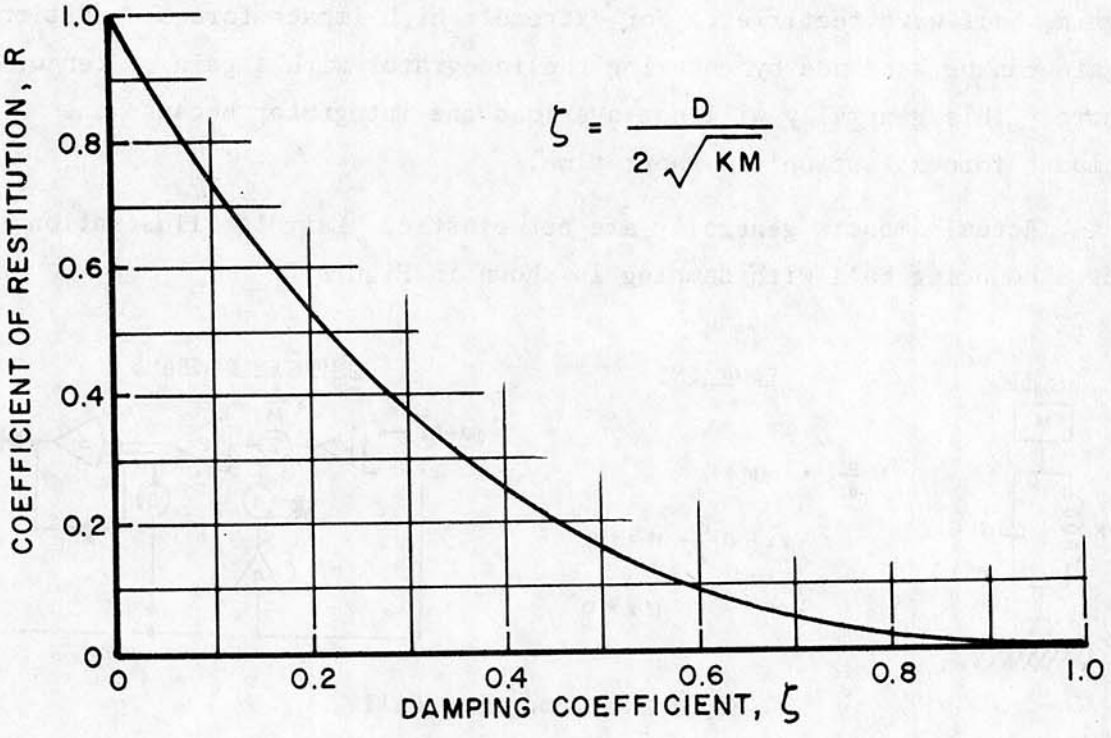

Figure 8. Coefficient of Restitution vs Damping Coefficient

In the M16 Rifle the collisions are between two moving masses rather than between one mass and a solid stop. The question arises immediately -- Can Figure 8 and equation (2) be used to calculate D for a two-body problem, given the coefficient of restitution R? To answer this, consider the two moving masses shown in Figure 9.

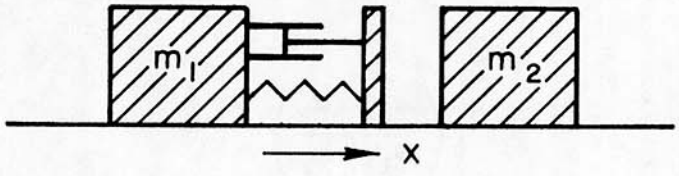

Figure 9. Damped Impact Between Two Masses

Note that external forces due, for example, to springs or to friction are not shown because they do not change appreciably during the very short time of the impact. The momentum of the system consisting of m_1 and m_2 is, therefore, conserved during the impact. The deformation force can be modeled as the sum of an elastic and a viscous force.

The equations of motion are then:

$$m_1 \ddot{x}_1 = -k\varepsilon - D\dot{\varepsilon} \tag{3}$$

where $k\varepsilon$ = the deformation force, $D\dot{\varepsilon}$ = the damping force,

$$\varepsilon = \begin{cases} x_1 - x_2 , & (x_1 - x_2) \geq 0 \\ 0 & (x_1 - x_2) < 0 \end{cases} , \text{ and} \tag{4}$$

$$m_2 \ddot{x}_2 = k\varepsilon + D\dot{\varepsilon} . \tag{5}$$

Combining (3) and (5):

$$\ddot{x}_2 = -\frac{m_1}{m_2} \ddot{x}_1 \tag{6}$$

and from (4):

$$\ddot{\varepsilon} = \begin{cases} \ddot{x}_1 - \ddot{x}_2 , & (x_1 - x_2) \geq 0 \\ 0 , & (x_1 - x_2) < 0 \end{cases} , \text{ or} \tag{7}$$

$$\ddot{\varepsilon} = \ddot{x}_1 \left(1 + \frac{m_1}{m_2}\right), \text{ from (6).} \tag{8}$$

Combining (3) and (8) gives:

$$\left(\frac{m_1 \quad m_2}{m_1 + m_2}\right)\ddot{\varepsilon} + D\dot{\varepsilon} + k\varepsilon = 0. \tag{9}$$

Now equation (9) is analogous to equation (1), so that the relation between R and D shown in Figure 8 can be used for two masses, provided the reduced mass--

$$\left(\frac{m_1 \quad m_2}{m_1 + m_2}\right)$$

is substituted for the actual mass.

Typical computer diagrams for the two-body problem are shown in Figure 10.

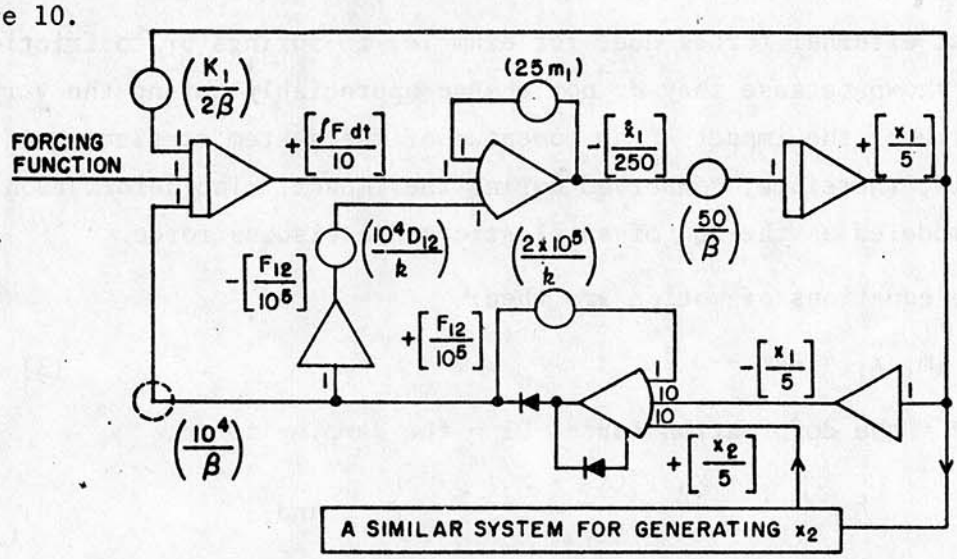

Figure 10. Analog Diagrams for Two-Body Impact

Note that the above diagram is somewhat different from that of Laird (Figure 7) in that the velocity is formed explicitly. This is done because in these simulations the velocity (or its sign) is used for controlling some of the comparators. In addition, the velocity is one of the desired computer outputs.

In neither circuit is the impact force generated explicitly. This is no great loss because the mathematical model is not sophisticated enough to yield accurately the large, short duration forces associated with impact.

An interesting simulation is the impact between a mass moving along a straight line and another mass that rotates about a fixed point, as shown in Figure 11.

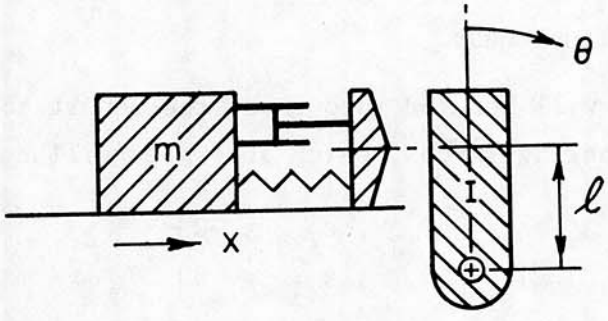

Figure 11. Combined Linear and Angular Impact

In the M16 rifle this problem is illustrated by the contact between the carrier and the hammer. As the carrier moves rearward it forces, or rotates, the hammer downward to its cocked position.

The equations of motion for Figure 11 are:

$$m\ddot{x} = -k\varepsilon - D\dot{\varepsilon}\ , \text{ and} \tag{10}$$

$$I\ddot{\theta} = (+k\varepsilon + D\dot{\varepsilon})\ \ell. \tag{11}$$

Thus:

$$m\ddot{x} = -\frac{I\ddot{\theta}}{\ell}\ ; \text{ also,} \tag{12}$$

$$\varepsilon = \begin{cases} x - \ell\theta, & (x - \ell\theta) \geq 0 \\ 0\ \ , & (x - \ell\theta) < 0 \end{cases} \tag{13}$$

and

$$\ddot{\varepsilon} = \begin{cases} \ddot{x} - \ell\ddot{\theta}, & (x - \ell\theta) \geq 0 \\ 0\ \ , & (x - \ell\theta) < 0 \end{cases} \tag{14}$$

so that, during impact,

$$\ddot{x} = \ddot{\varepsilon} + \ell\ \ddot{\theta}, \text{ or}$$

$$\ddot{x} = \ddot{\varepsilon}\left(\frac{I}{I + m\ell^2}\right), \text{ from (12).} \tag{15}$$

Equation (10) may then be written:

$$\left(\frac{I}{I + m\ell^2}\right) m\ddot{\varepsilon} + D\dot{\varepsilon} + k\varepsilon = 0. \qquad (16)$$

Again, (16) is like equation (1) with the reduced mass

$$\left(\frac{I}{I + m\ell^2}\right) m$$

substituted for the actual mass.

These techniques will be used throughout the report to simulate contact, impact and locking forces, which generally will be written:

$$F_{ij} = \begin{cases} k\varepsilon_{ij} , & \varepsilon_{ij} \geq 0 \\ 0 , & \varepsilon_{ij} < 0 \end{cases}.$$

Now it must be emphasized that this force is only the elastic component; there generally is a viscous component. However, to simplify the writing, these forces will be designated by the elastic component with the understanding that there is a viscous component, such that the coefficient of restitution is 0.5 unless specifically indicated to be otherwise.

IV. THE FORCES DUE TO PRESSURE

A. The Powder Pressure

Since the powder pressure is the primary force acting on the rifle mechanism it must be properly simulated. The powder pressure could be calculated by the usual methods of interior ballistics;[10] but for this study a measured pressure-time curve was used to insure that it (the input to the simulation) was consistent with the simultaneously measured displacement-time curves to which the output of the simulation will be compared.

Usually the pressure-time curve is simulated in the analog computer by a diode function generator. It has been found that the output of the diode function generator is not consistent and another technique was devised.[11]

The basic idea of the technique is that a very good representation of a given curve can be obtained by integrating a rough approximation of the derivative of that curve. The derivative of the first part of the pressure-time curve was approximated by a triangle generated by amplifiers 126 and 127 of Figure 12.

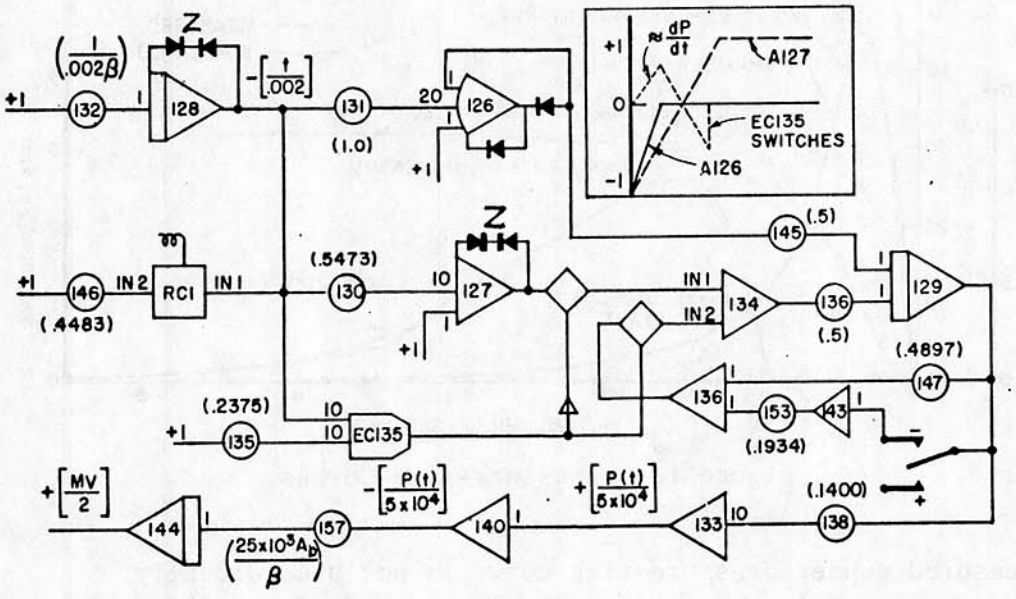

Figure 12. Circuits for Generating the Powder Pressure-Time Curve

The derivative was integrated to a point after maximum pressure by integrator 129. At that point electronic comparator 135 switches and changes the path of the input to 129, thereby inserting resistance (potentiometer 147) in the feedback so that the integral (the pressure-time curve) decays exponentially to zero. At a later time (t=.9ms) the rate of decay was changed by reducing the resistance (pot 153) in the feedback.

Comparisons of the simulated and the measured pressure-time curves are shown in Figure 13.

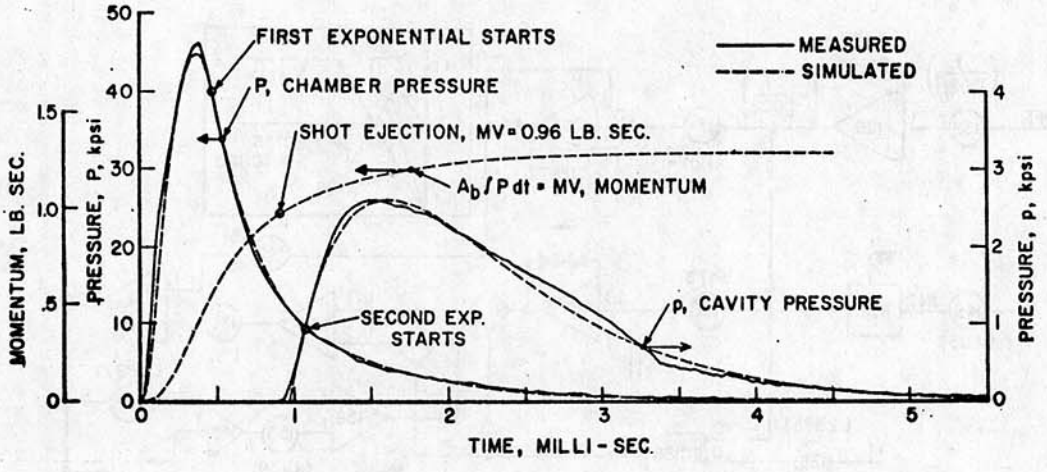

Figure 13. Pressure-Time Curves

The measured powder pressure-time curve is not used directly as the forcing function because the rearward force acting at the chamber is opposed by the forward-acting friction forces between the bore surface and the projectile and gas. These friction forces are not known in detail, but the momentum of the projectile and powder gas at the instant of shot ejection is known; i.e.,

$$\left(W_{\text{projectile}} + \frac{W_{\text{charge}}}{2}\right) V_{\text{projectile}} .$$

This known value, together with the area of the bore, was used to normalize the integral of the pressure-time curve and thereby establish the scale of force (and powder pressure) to be used in the recoil problem.

B. The Carrier Cavity Pressure

Methods for calculating the pressure in the carrier cavity are described in other Ballistic Research Laboratories reports.[3,4] In this report the cavity pressure is obtained empirically from the powder pressure in the chamber. The circuits for the cavity pressure are shown in Figure 14.

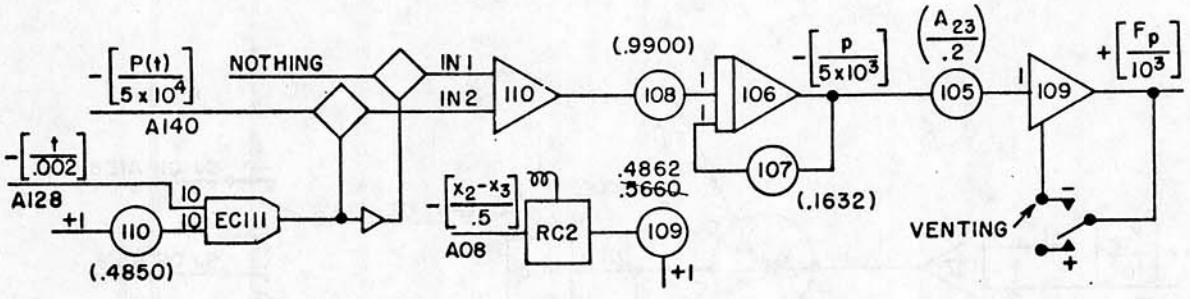

Figure 14. Circuits for Generating the Pressure in the Carrier Cavity

The circuits are like the physical situation in that EC111 "holds off" the pressure for a time corresponding to the travel of the projectile to the gas port and the transit of the gas to the cavity. Losses and amplitude scaling are represented by pots 107 and 108. It must not be inferred that this circuit could be used a priori to calculate (or simulate) the cavity pressure. The circuit is empirical; the pots were set by trial to match the measured curve. The curve shown in Figure 13 was used.

It should be noted in Figure 14 that the cavity pressure is suddenly reduced to zero at the instant of unlocking by RC 2. This simulates the bolt striking the limit stop in the carrier so that

the cavity pressure can no longer have any external effect. (The limit stop is approximatly 0.04 inches beyond the unlocked position, but it was not practical to use that limit force, F_{zb}, to switch off the pressure because the bolt can rebound between the stop and the top of the cam path.)

C. The Control Circuit for the Pressures

When the hammer strikes the firing pin, it moves forward, strikes the primer and fires the cartridge. In this simulation, the impact of the hammer on the firing pin produces F_θ which is used to trigger SCR1, as shown in Figure 15.

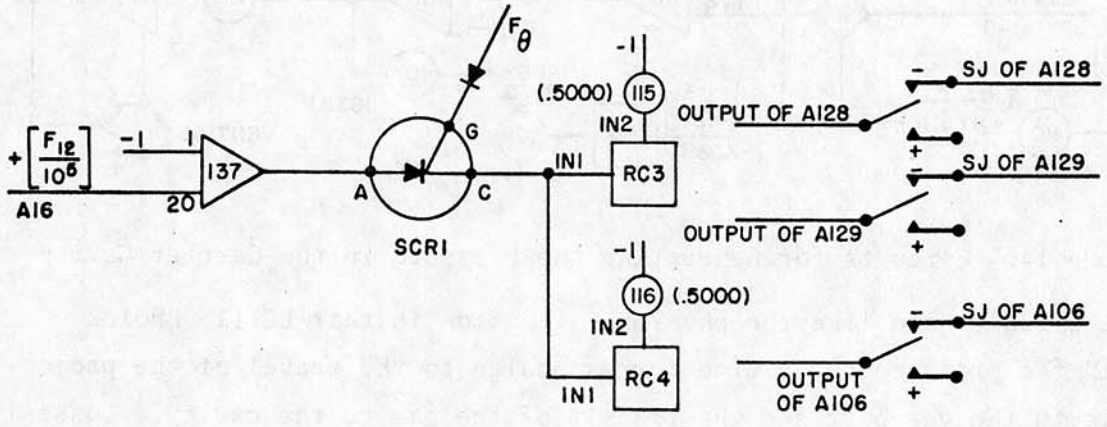

Figure 15. Control Circuits

The current passed by SCR1 actuates relay comparators RC3 and RC4, removing the short circuit on amplifiers 128, 129, and 106 (see Figures 12 and 14). This starts the pressure-time curves.

The relay comparators RC3 and RC4 are reset (de-activated) by "breaking" the input voltage to the SCR. This is produced by the negative voltage, $-F_{12}$, generated when the carrier strikes the gun upon return to battery. The circuit is thus ready for the second shot when the hammer strikes the firing pin.

V. THE BOLT MOTION

A. The Linear Motion

In writing the equations of motion for the various components, their position at the instant of firing will be taken as the origin, as indicated in Figure 16.

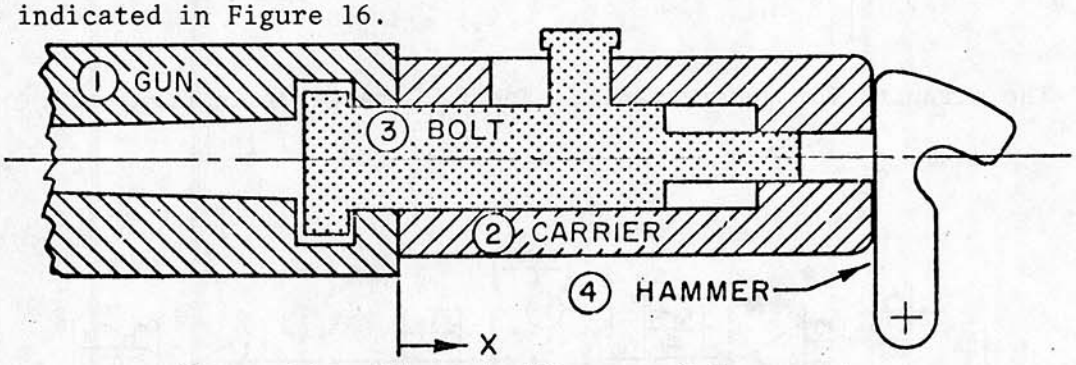

Figure 16. Schematic Diagram of Components

The acceleration of the bolt, $\ddot{x}_3$, is equal to the sum of the forces acting upon it divided by the mass of the bolt, m_3. The forces acting on the bolt are:

- powder pressure force, $+F_{p3} = pA_1$;
- cavity pressure force, $-F_p = -pA_{23}$;
- locking force with gun, $+F_{13}$ and $-F_{31}$;
- cam force, $-F_z$;
- limit stop forces, $-F_{az}$ and $+F_{zb}$.

The pressure forces are straightforward and are obtained from the circuits of Figure 12 and Figure 14.

The contact forces are given by:

$$F_{31} = k\varepsilon_{31}, \text{ where}$$

$$\varepsilon_{31} = \begin{cases} (x_3 - x_1) - \Delta, & (x_3 - x_1) - \Delta \geq 0 \\ 0, & (x_3 - x_1) - \Delta < 0 \end{cases}$$

Δ = clearance, (0.003 in.)

Likewise,

$$F_{13} = k\varepsilon_{13}$$

$$\varepsilon_{13} = \begin{cases} (x_1 - x_3) - \Delta, & (x_1 - x_3) - \Delta \geq 0 \\ 0, & (x_1 - x_3) - \Delta < 0 \end{cases}.$$

The circuits for generating F_{13} and F_{31} are given in Figure 17.

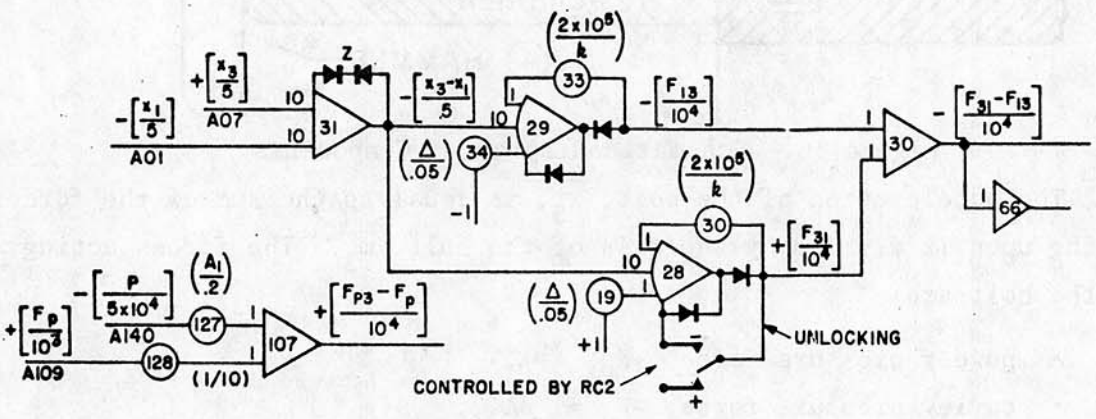

Figure 17. Circuits for Generating the Locking Force

Note that when the bolt becomes unlocked, amplifier 29 (F_{13}) is short-circuited by relay comparator RC2 so that there is no force between the gun and the rear surface of the bolt lugs.

The cam force and the limit stop forces are described in the next section of the report.

The main loop for calculating the motion of the bolt is given in Figure 18.

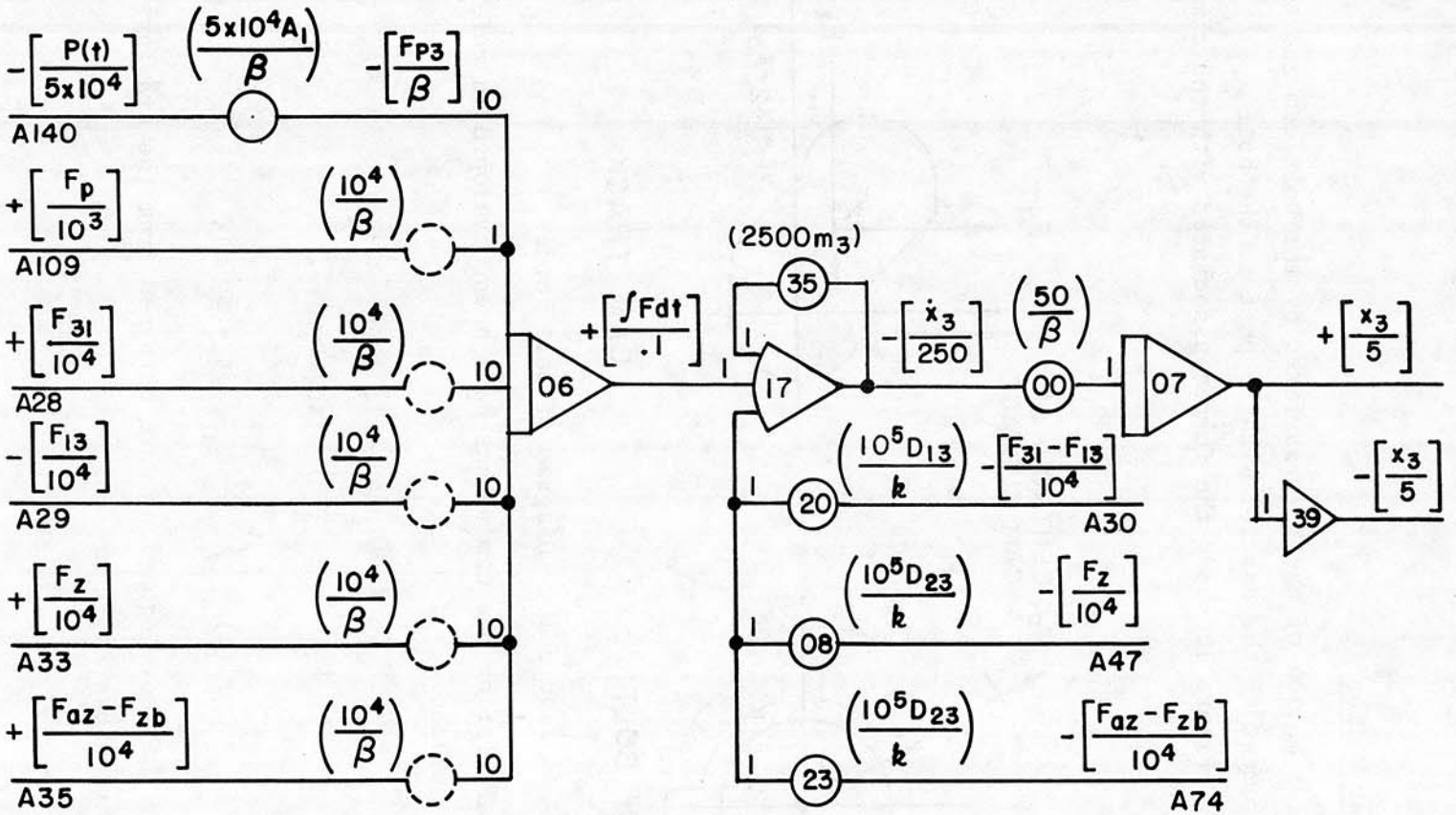

Figure 18. Circuits for Calculating the Linear Motion of the Bolt

B. The Angular Motion

The angular motion of the bolt is fixed by the bolt cam and the linear displacement of the carrier with respect to the bolt, $(x_2 - x_3) = z$. Figure 19 shows the forces associated with the cam.

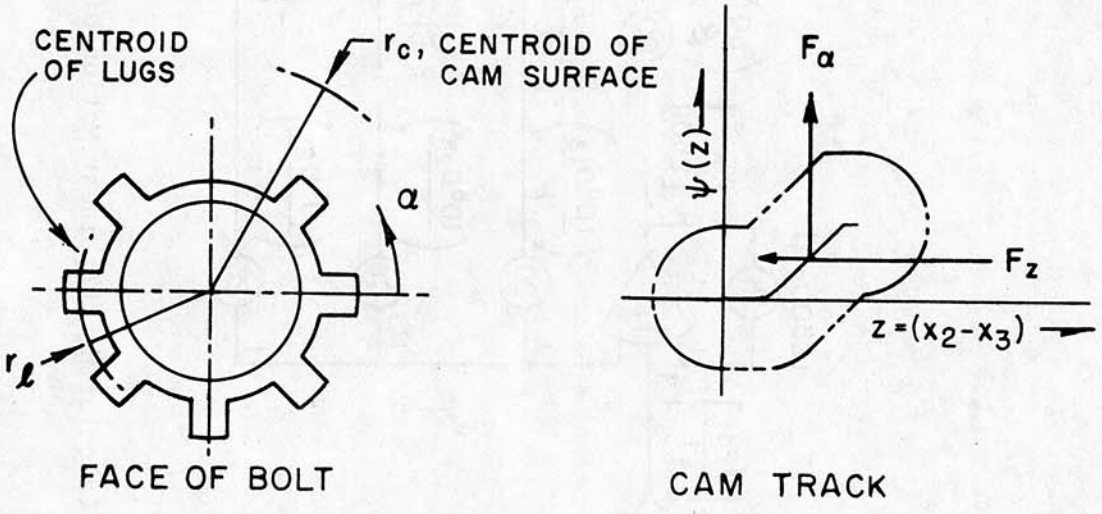

Figure 19. Diagram of Bolt Forces

Methods for calculating the cam forces have been developed in reference 12. By those methods:

$$F_\alpha = k \ [\alpha - \psi(z)], \text{ and}$$

$$F_z = - F_\alpha \frac{d\alpha}{dz} \text{ ; also}$$

$$\psi(z) = \int_0^t \frac{d\alpha}{dz} \frac{dz}{dt} \, dt + \psi(0).$$

Input data for the above equations were obtained from the drawings of the cam, and are shown in Figure 20.

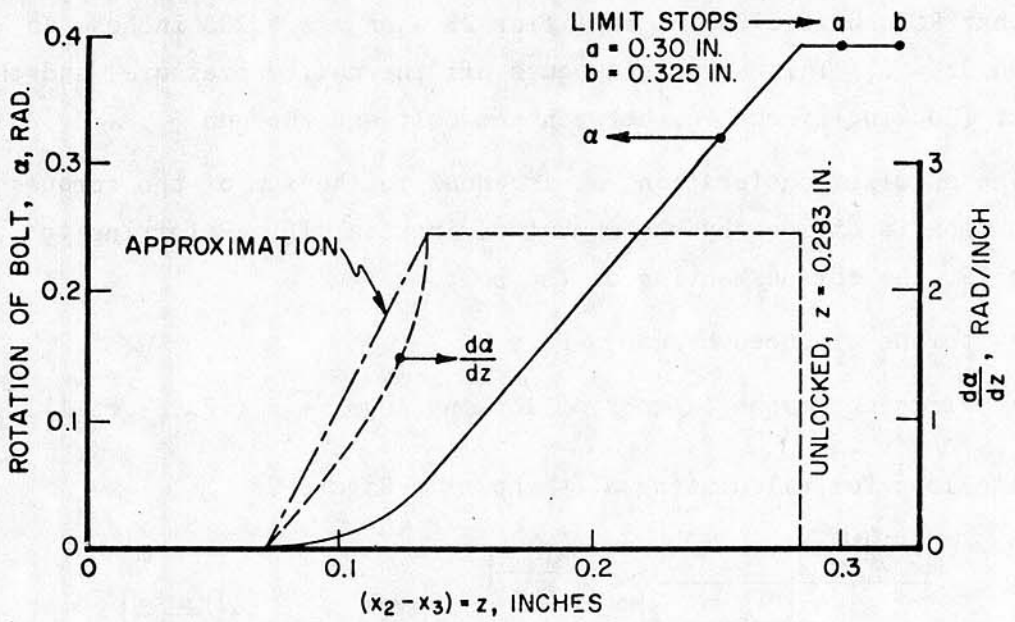

Figure 20. The Cam Track and Its Derivative

The analog circuits for generating F_α and F_z are shown in Figure 21.

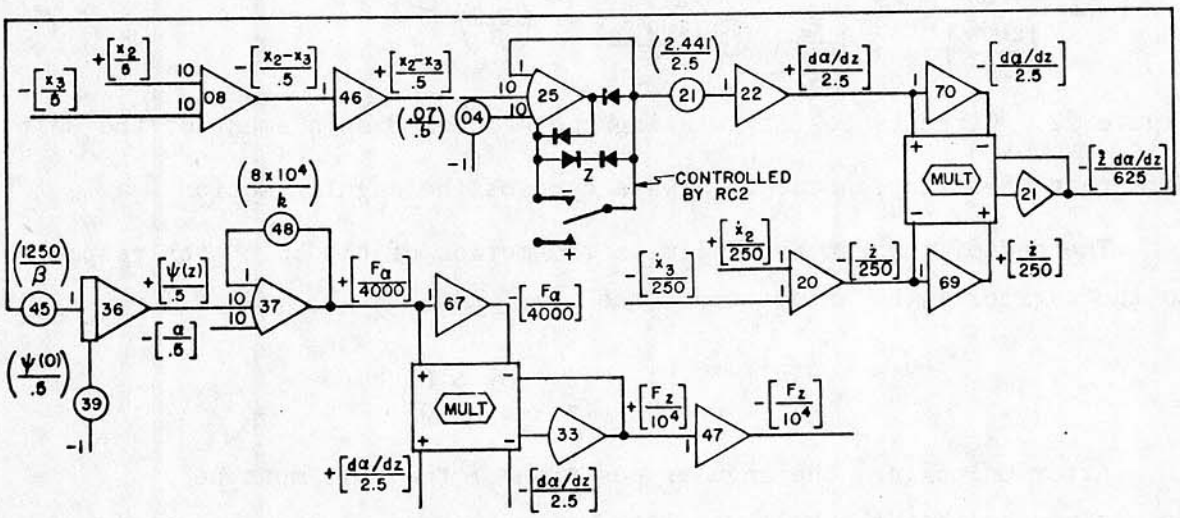

Figure 21. Circuits for Generating F_α and F_z

Note that RC2 short-circuits amplifier 25 when z = 0.283 inches, so that $d\alpha/dz = 0$. This same relay cuts off the cavity pressure, and the contact (locking) force F_{31} between the bolt and the gun.

The angular acceleration, $\ddot{\alpha}$, is equal to the sum of the torques acting upon it divided by the moment of inertia, I_3. Referring to Figure 19, the torques acting on the bolt are:

- torque produced by cam, $-F_\alpha \, r_c$
- friction torque on ends of locking lugs, $\mp \mu \, (|F_{31} - F_{13}|) \, r_\ell$.

The loop for calculating α is shown in Figure 22.

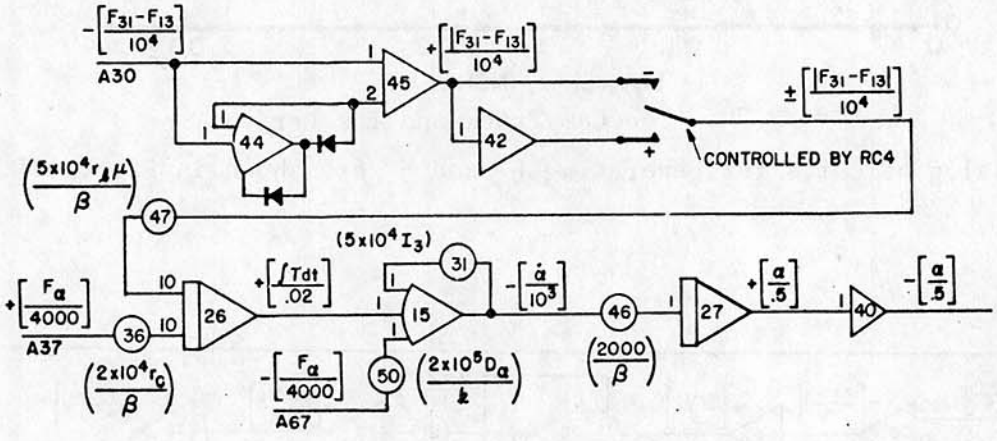

Figure 22. Circuits for Calculating the Angular Displacement of the Bolt

Note that the friction torque always opposes the angular motion.

The end of the cam track limits the motion of the bolt with respect to the carrier. The associated force is: (see figure 20)

$$F_{zb} = \begin{cases} k\,(z - b), & (z - b) \geq 0 \\ 0 & (z - b) < 0 \end{cases}.$$

After unlocking, the angular position of the bolt must be maintained so that the bolt can lock-up again when it and the carrier return to battery. In the rifle this is done by engaging the head of the bolt cam pin in a slot in the receiver (gun). The slot begins at 0.405 inches rearward of the battery position of the carrier. To simulate the linear force imposed by this restraint (i.e., the

impact of the pin on the topmost slanted part of the cam track) a limit stop force is introduced at z = a; see Figure 20. This force is:

$$F_{az} = \begin{cases} k\,(a - z), & (a - z) \geq 0,\ \dot{z} < 0 \\ 0, & (a - z) < 0 \\ 0, & (x_2 - x_1) < 0.405 \text{ in.} \end{cases}.$$

Figure 23 gives the circuits for generating these forces.

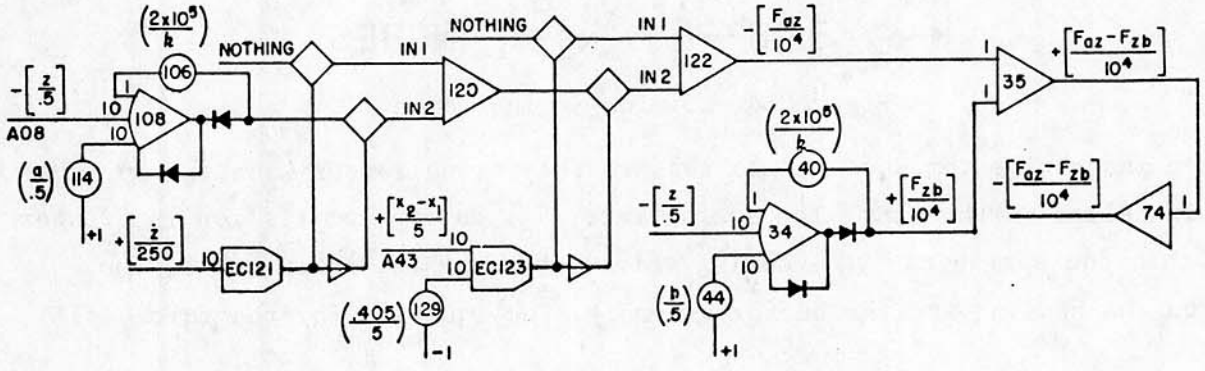

Figure 23. Circuits for Generating the Limit Stop Forces

VI. THE CARRIER MOTION

The acceleration of the carrier, $\ddot{x}_2$, is equal to the sum of the forces acting upon it divided by the mass of the carrier, m_2. The forces acting on the carrier are:

- cavity pressure force, $+F_p$;
- bolt cam force, $+F_z$;
- bolt cam limit stop forces, $+F_{az}$ and $-F_{zb}$;

- driving spring force, $-F_D$;
- contact force with gun, $+F_{12}$;
- buffer force, $-F_B$;
- hammer contact force, $-F_{24}$.

The first four forces above have been given previously. The driving spring force is illustrated in Figure 24.

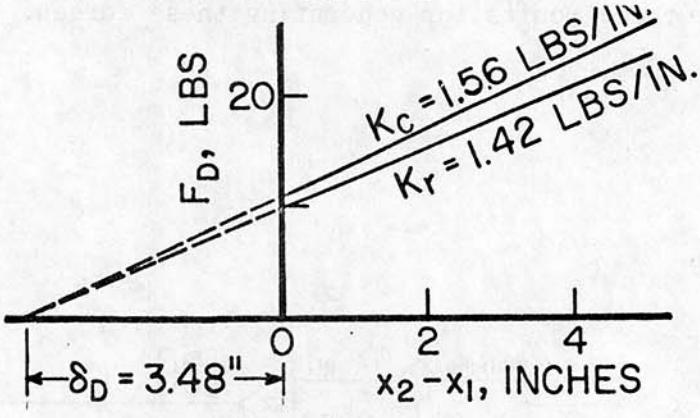

Figure 24. Driving Spring Force

An Instron Tester was used to measure the spring forces with the spring installed in the gun. The spring rate, K_c, during compression is greater than the spring rate, K_r, during release because the spring coils rub on the housing and the buffer assembly. The equation for the force is:

$$F_D = \begin{cases} K_c & (\delta_D + x_2 - x_1),\ (\dot{x}_2 - \dot{x}_1) \geq 0 \\ K_r & (\delta_D + x_2 - x_1),\ (\dot{x}_2 - \dot{x}_1) < 0 \end{cases}.$$

The circuits for generating F_D are shown in Figure 25.

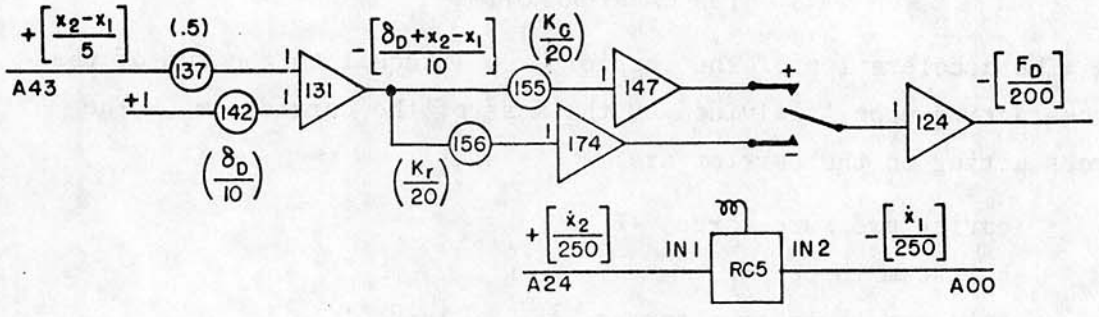

Figure 25. Circuits for Generating the Driving Spring Force

The contact force, F_{12}, between the gun and the carrier, stops the carrier at battery position. It is:

$$F_{12} = \begin{cases} k\ (x_1 - x_2) & , (x_1 - x_2) \geq 0 \\ 0 & , (x_1 - x_2) < 0 \end{cases}.$$

The buffer is considered to act like a spring with damping. Compression tests of the polyurethane buffer button indicated that its spring rate, K_B, was approximately 5000 pounds per inch. The elastic part of the buffer force is then given by:

$$F_B = \begin{cases} K_B\ (x_2 - x_1 - \delta_B), & (x_2 - x_1 - \delta_B) \geq 0 \\ 0 & , (x_2 - x_1 - \delta_B) < 0 \end{cases}.$$

The velocities observed before and after impact on the buffer indicated that the coefficient of restitution, R, was 0.47. The damping coefficient, D_B, calculated as outlined under "Contact Forces", was 1.63 lb. sec/in. The circuits for generating F_{12} and F_B are given in Figure 26.

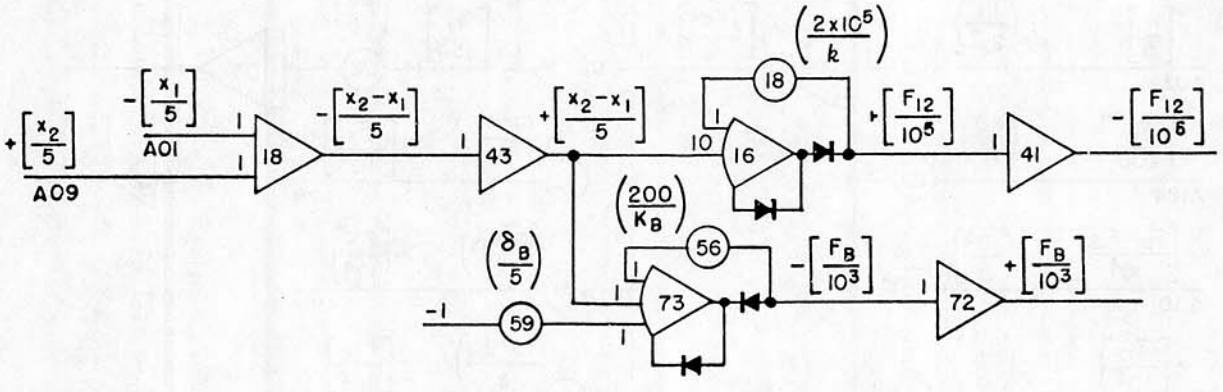

Figure 26. Circuits for Generating F_{12} and F_B

The hammer contact force, F_{24}, will be described later in the report.

The main computing loop for the carrier is shown in Figure 27.

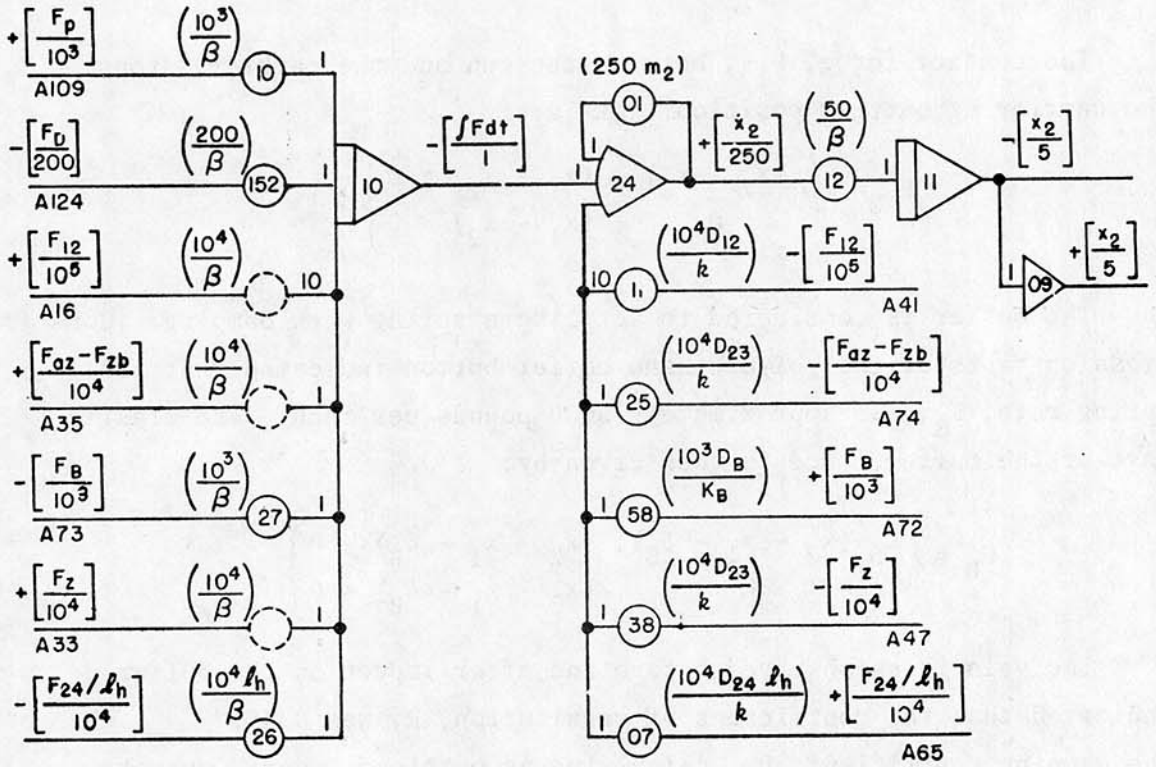

Figure 27. Circuits for Calculating the Carrier Motion

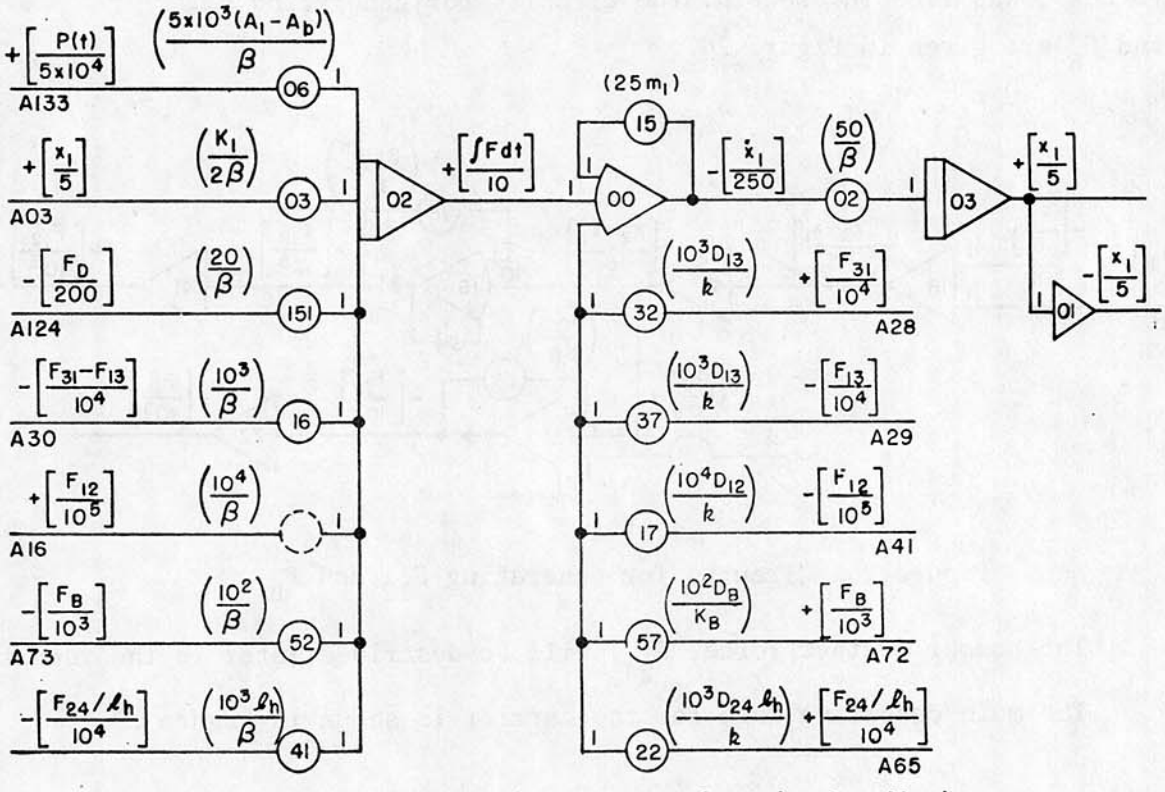

Figure 28. Circuits for Calculating the Gun Motion

VII. THE GUN MOTION

The acceleration of the gun, $\ddot{x}_1$, is equal to the sum of the forces acting on it divided by the mass of the gun, m_1. The forces acting on the gun are:

- powder pressure force, $-F_{P1} = -P\ (A_1 - A_b)$;
- locking force with bolt, $-F_{13}$ and $+F_{31}$;
- contact force with carrier, $-F_{12}$;
- driving spring force, $+F_D$;
- buffer force, $+F_B$;
- recoil spring force, $-F_R$;
- hammer contact force, $+F_{24}$.

All of the above forces have been defined except the last two. The experimental mounting of the gun had practically no friction, as mentioned previously (see Figure 1), so that the recoil spring force is:

$$F_R = K_1\ x_1.$$

The computing loop is shown in Figure 28.

VIII. THE HAMMER MOTION

At the beginning of this study the dynamics of a hammer were not modeled. Although hammers are almost universal in hand guns, they generally are not used in automatic weapons. The forward swing of the hammer was important because it introduces a "delay" in the firing cycle, but this motion can be calculated in the straightforward manner. To provide data, the forward swing and rebound of the hammer were recorded (with an empty chamber) but data were not obtained during a firing test mainly because of the difficulty of attaching to the hammer a reflector that could be seen, or some other device.

Early results on the computer indicated that the simulated carrier motion was faster than the measured motion. The observed retardation was much greater than could be reasonably attributed to friction

between the carrier and/or the driving spring and the receiver. Also, no magazine was used in the single-shot experiments, so that there was no friction between the carrier and the incoming round. However, the camming and rubbing actions between the carrier and the hammer can produce the slower motion of the carrier, as indicated by the wear marks on the bottom of the carrier.

The initial forward swing of the hammer is simple harmonic motion and is easily simulated. The impact of the firing pin, was (in this simulation) at first on the carrier. However, this did not produce consistent results because the equilibration of the initial driving spring force between the carrier and the gun by F_{12} caused a "jitter" in the carrier as the hammer moved forward. The rebound of the hammer was affected by the jitter. To eliminate this effect the impact was "moved" to a solid stop, and the impact torque was:

$$T_\theta = \begin{cases} -K\theta, & \theta \leq 0 \\ 0, & \theta > 0 \end{cases}, \text{ where}$$

K = a high torsional spring rate, in. lb/rad.

The damping coefficient was calculated to be: $D_\theta = 2.765$, corresponding to the observed coefficient of restitution of 0.7. Note that T_θ triggers the pressure-time curve (see Figure 15).

The subsequent interaction between the hammer and the carrier is illustrated in Figure 29. In writing the equation of motion for the hammer, the point, O, will be assumed to be fixed. However, point O accelerates with the gun so that an additional torque, T_g, should be applied to the hammer. The torque is:

$$T_g = -m_4 \ddot{x}_1 \lambda \cos\theta, \text{ where}$$

λ = distance from O to CG, see Figure 29.

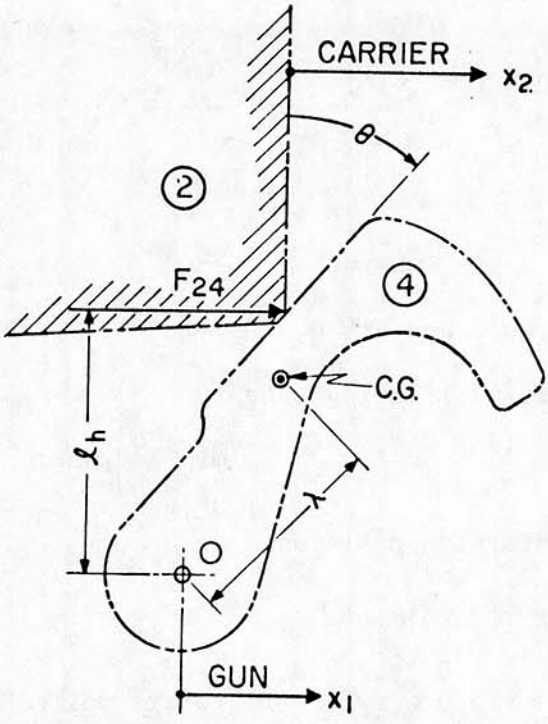

Figure 29. Carrier-Hammer Diagram

The omission of T_g is most serious during the time the powder pressure acts ($\ddot{x}_1$ is large). Its main effect is thus on the rebound of the hammer. Now the impact of the hammer is: on the firing pin, to the primer, to the cartridge case, to the gun. The rebound from all of these parts can be further complicated by a large rearward force on the firing pin due to setback of the primer cup. In view of these complications and the lack of measured motion of the hammer and the instabilities in the analog circuits mentioned previously, the torque, T_g, will be omitted.

The angular acceleration of the hammer, $\ddot{\theta}$, is equal to the sum of the torques acting upon it divided by the moment of inertia, I_4. The torques acting on the hammer are:

- spring torque, $-T_s$;
- impact torque, $+T_\theta$;
- limit stop torque, $-T_m$;
- latching torque, $+T_\ell$;
- contact torque with carrier, $+T_{24}$.

The initial conditions are:

$\theta(0) = 1.065$ rad $(61°)$

$\dot{\theta}(0) = 0.$

The torques are:

$T_s = T_o + \underline{K}\,\theta$, where

T_o = torque when $\theta = 0$,

$\underline{K}$ = torsional spring rate.

$$T_m = \begin{cases} K\,(\theta - \theta_m), & (\theta - \theta_m) \geq 0 \\ 0, & (\theta - \theta_m) < 0 \end{cases} \text{ where}$$

θ_m = limit stop position.

$$T_\ell = \begin{cases} K\,(\theta_\ell - \theta), \ \theta \leq \theta_\ell, \ \dot{\theta} < 0, \\ 0, \ \theta > \theta_\ell, \\ 0, \text{ when trigger is pulled} \end{cases}.$$

Note that T_m and T_ℓ do not react on any other part. Since θ is roughly $65°$ when T_m and T_ℓ take place, the horizontal component of the associated torques are small and would have little effect on the horizontal motion of the much heavier gun. The circuits for generating these torques are shown in Figure 30.

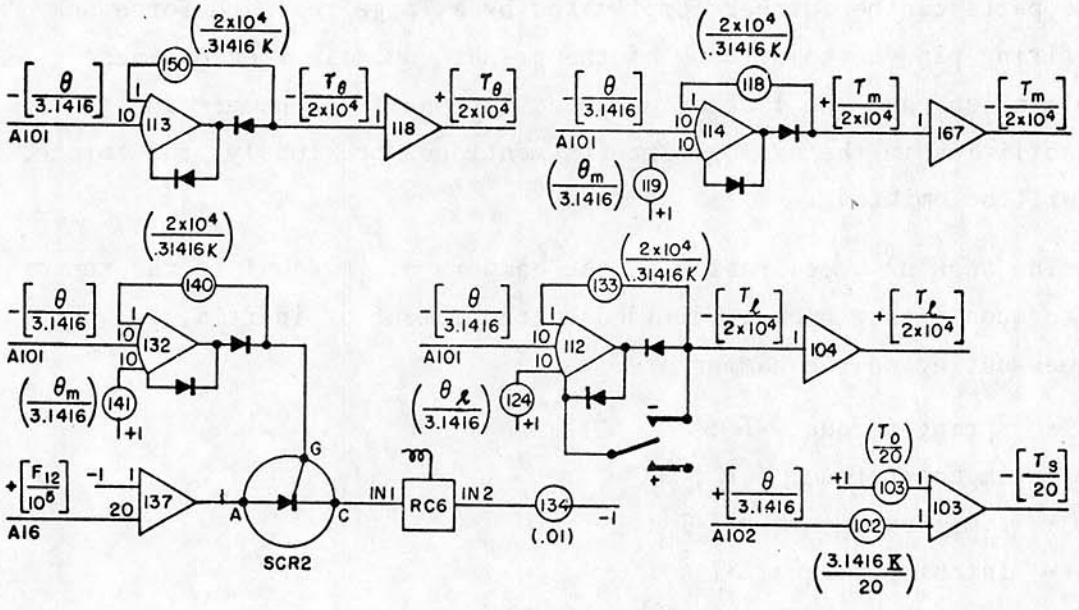

Figure 30. Circuits for Generating the Torques on the Hammer

The contact torque with the carrier is:

$$T_{24} = |F_{24}|\ \ell_h,\ T_{24} \geq 0, \text{ where}$$

ℓ_h = distance from hammer pivot to carrier; see Figure 29.

$$F_{24} = \begin{cases} +k\ell_h\varepsilon_{24}, & (\dot{x}_2 - \dot{x}_1) \geq 0 \\ -k\ell_h\varepsilon_{24}, & (\dot{x}_2 - \dot{x}_1) < 0 \end{cases}$$

$$\varepsilon_{24} = \begin{cases} [\phi\ (x_2 - x_1) - \theta]\ \ell_h, & [\phi(x_2 - x_1) - \theta] \geq 0 \\ 0 & [\phi(x_2 - x_1) - \theta] < 0 \end{cases}.$$

The measured rotation of the hammer vs displacement of the carrier, shown in Figure 31, is the basis of $\phi(x_2 - x_1)$.

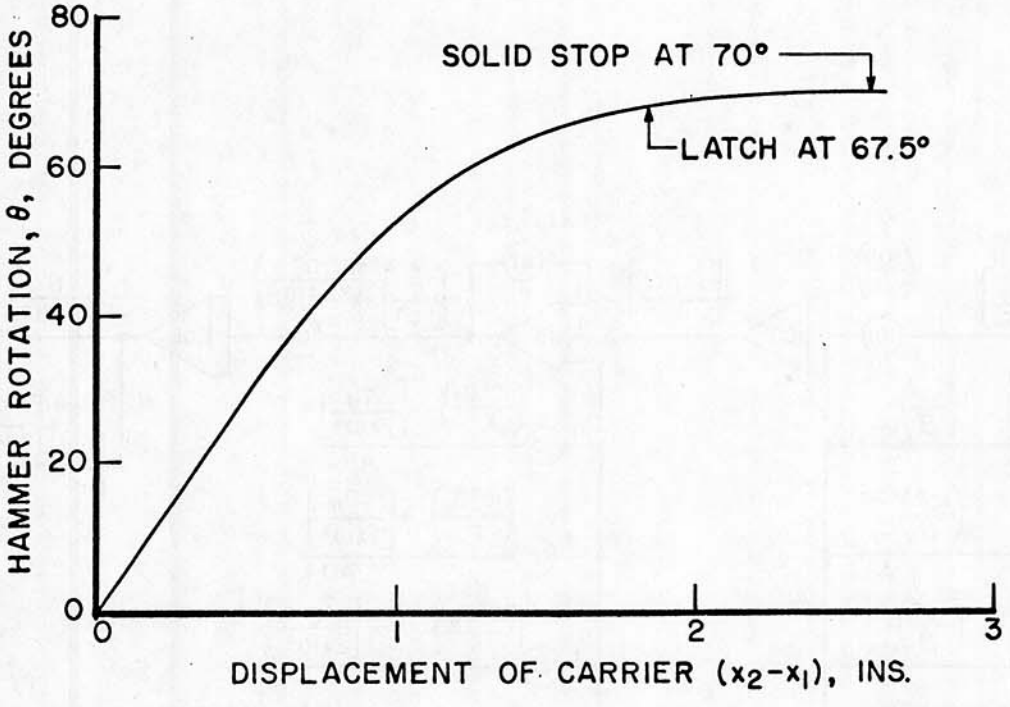

Figure 31. Hammer Rotation vs Carrier Displacement

The circuits for generating the hammer-carrier force, F_{24}, are shown in Figure 32.

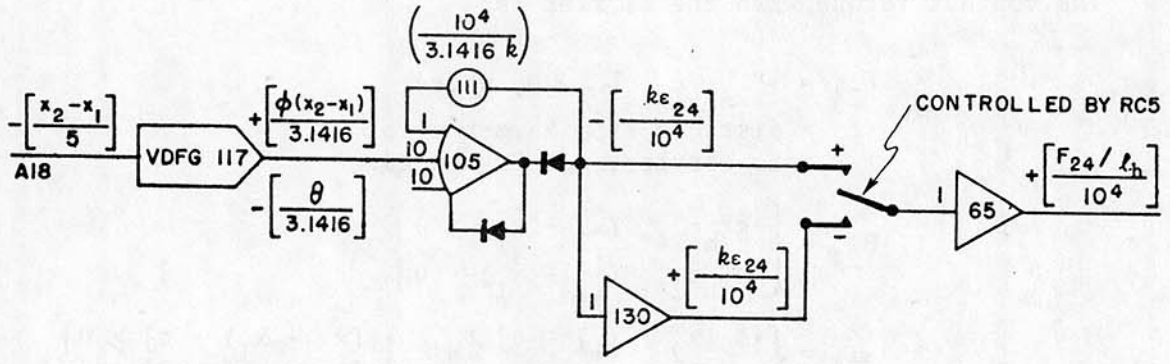

Figure 32. Circuits for Generating the Hammer-Carrier Force

The loop for calculating the motion of the hammer is shown in Figure 33.

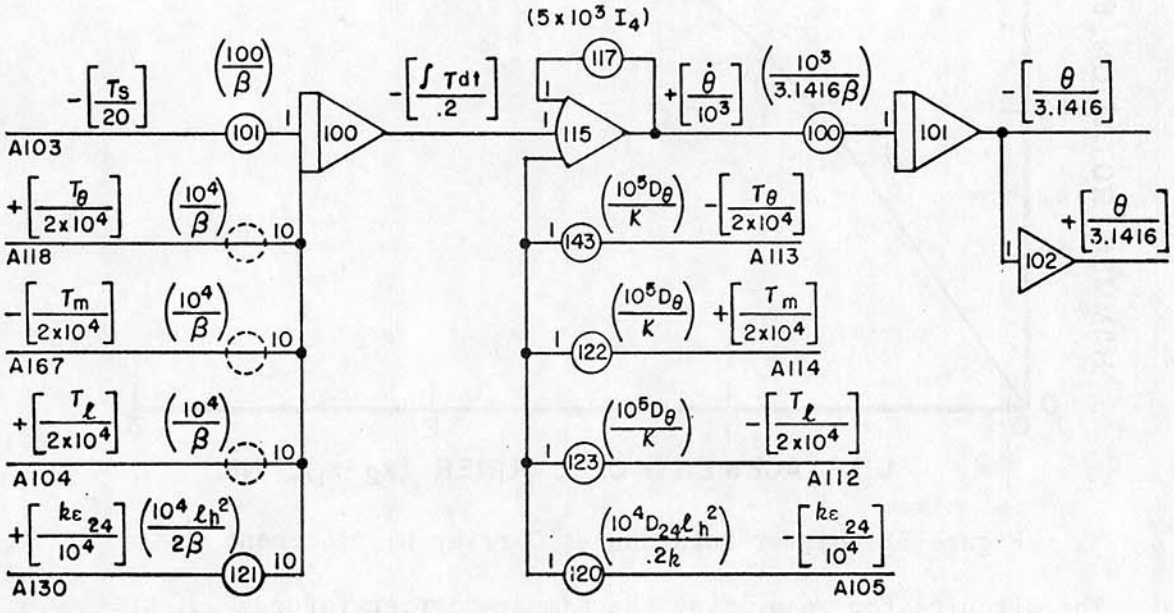

Figure 33. Circuits for Calculating the Angular Displacement of the Hammer

IX. RESULTS

The final result, or calculated motion of the components, is illustrated in Figure 34.

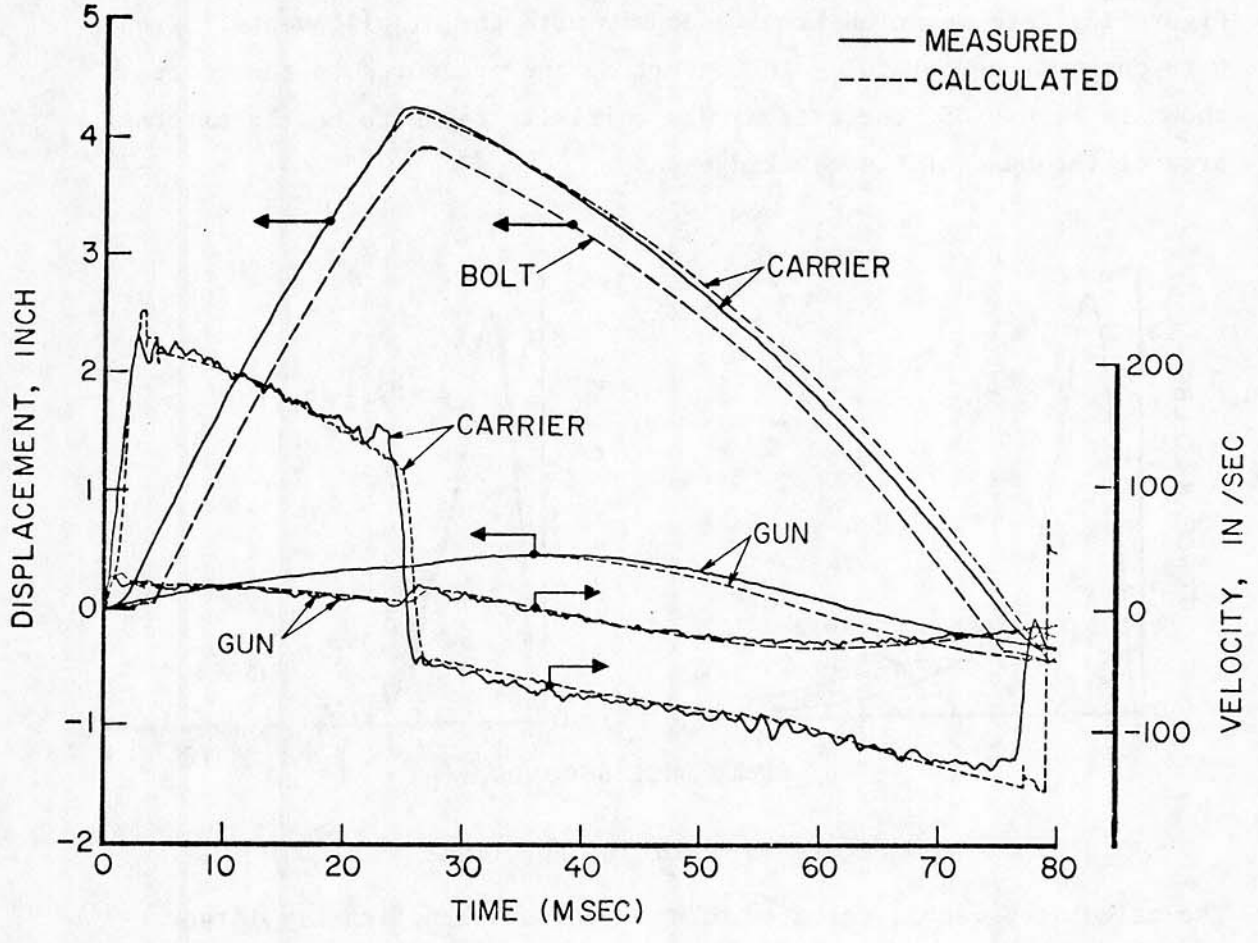

Figure 34. Displacements and Velocities vs Time

The agreement between the measured and the calculated motion is quite good, lending credence to the mathematical model of the gun mechanism.

Now it must be emphasized that one should not expect the very good agreement shown in Figure 34 to be obtained by use of a priori methods alone. To obtain these results, some of our first concepts of the model and several of the parameters were revised. The revisions generally were not drastic, mainly reflecting our lack of knowledge or experience

in evaluating losses such as inelastic impact and friction. However, it is those revisions that are important in advancing our ability to devise more realistic models, and they will be discussed in some detail.

A prime reason for the good agreement is that the pressures (see Figure 13) were measured simultaneously with the displacements. Even here one must be careful. In converting the pressures to the forces shown in Figure 35, the area A_1 was initially taken to be the external area of the base of the cartridge case.

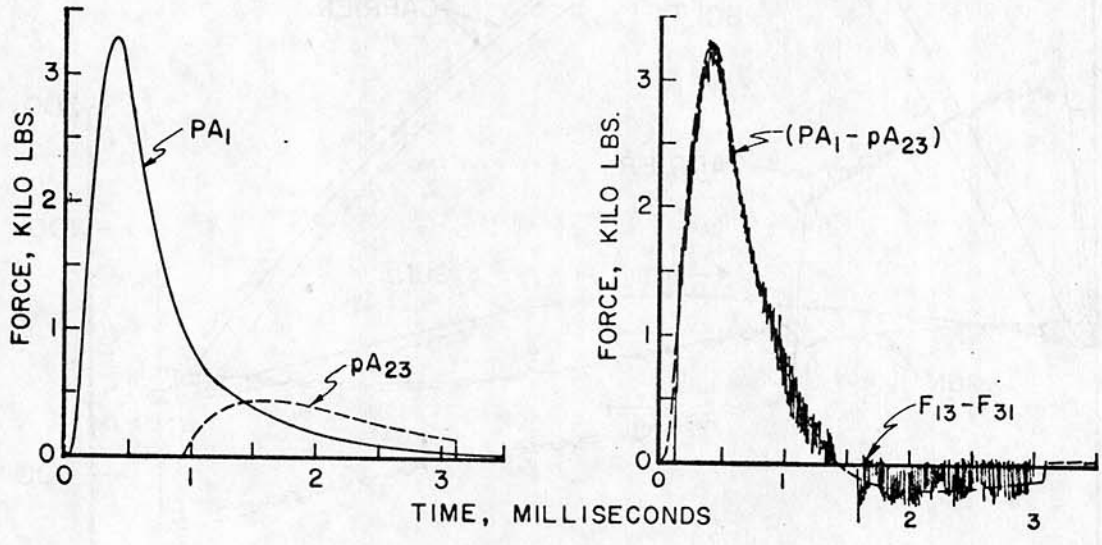

Figure 35. Forcing Functions

The calculated recoil velocity of the gun was significantly larger than that measured; when A_1 was changed to the internal area of the base of the case, (i.e., the proper value) the agreement was adequate as shown. Also, the calculated velocity of the carrier continued to increase for a longer time than did the measured velocity. It was then realized that when the bolt cam pin strikes the end of the cam track in the carrier, the cavity pressure produces only an internal force between the bolt and the carrier, and thus has no effect on their motion. Therefore, the carrier force was reduced to zero at the proper displacement by RC2 of Figure 14. The corresponding time was

approximately 3.1 milliseconds, as shown in Figure 35.

The net force ($PA_1 - pA_{23}$) acting on the bolt is shown at the right of Figure 35. Note that after about 1.5 milliseconds the force is negative; i.e., the bolt tends to move into the chamber, because the much larger area of the bolt cavity "magnifies" the cavity pressure. The net force acting on the bolt is transmitted to the barrel by the contact force (F_{13}-F_{31}), so that the two forces should be equal when the bolt is locked to the barrel. The agreement is illustrated in Figure 35. As pointed out in "Contact Forces," ($F_{13} - F_{31}$) is only the elastic part of the contact force because the viscous part is not generated explicitly in the analog circuits. The rapid oscillatory nature of the contact force is to be expected because it is generated by impact. On the average, the agreement is very good.

The initial velocities are shown in Figure 36.

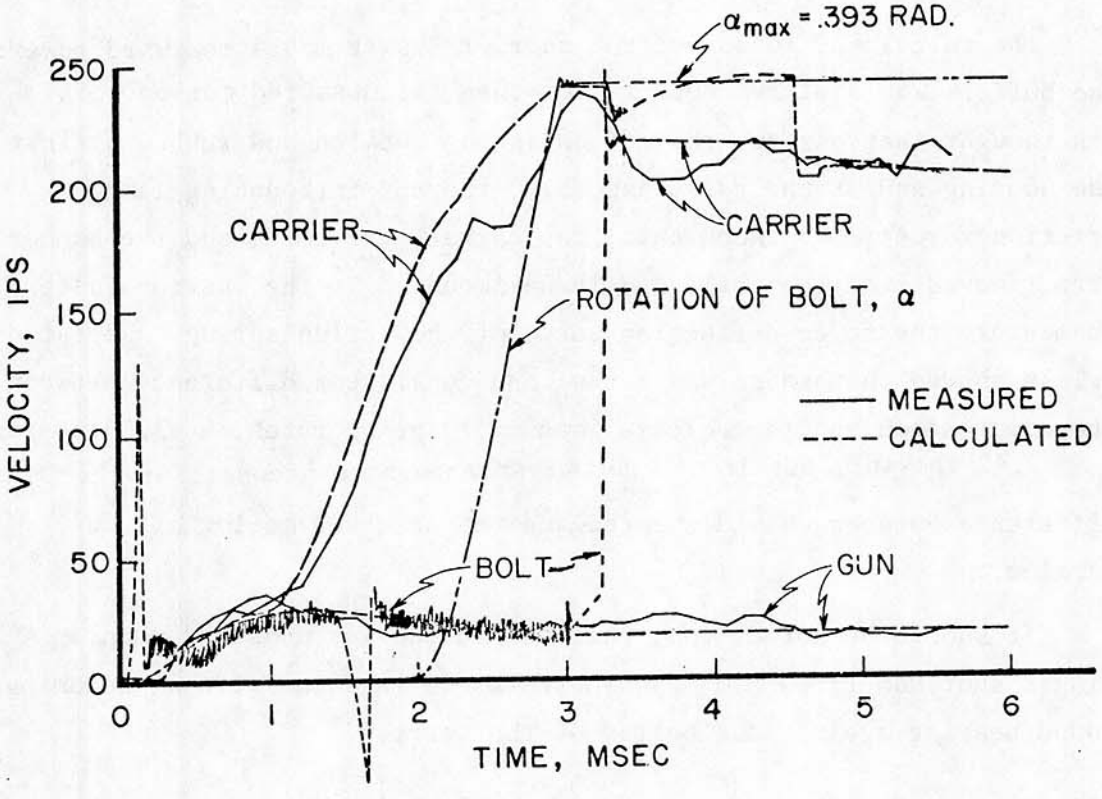

Figure 36. Initial Velocities

The velocity of the bolt is very rough because it oscillates through the clearance between the bolt lugs and the barrel (gun). The initial, very large spike in the bolt velocity is due to the applied powder pressure; it is immediately reduced by the bolt reacting on the gun and carrier, moving them rearward. The second (negative) spike in the bolt velocity curve takes place as the applied force changes sign (see Figure 35). At about one millisecond the carrier cavity pressure moves the carrier rearward with respect to the bolt. At two milliseconds the bolt begins to rotate, completing the rotation at about three milliseconds. When the unlocking is completed at about 3.1 milliseconds and the bolt cam pin strikes the end of the cam track, the bolt is "snatched" rearward by the carrier. After rebound, the bolt and carrier come together again at 4.5 milliseconds and travel rearward.

The calculated motion of the carrier, as it moves rearward toward the buffer, was at first much faster than the measured motion. It was thought that perhaps the action spring buckled and rubbed against the housing and/or the guide assembly, thereby introducing large friction forces. To check this, the barrel, the bolt, and the hammer were removed from the rifle and it was mounted in the Instron Tester to measure the force-deflection curve of the action spring. Repeated trials showed that there was a real and consistent difference between the compression and the release loads, or spring rates, K_c=1.56 lbs/in., K_r = 1.42 lbs/in., but it was not great enough to account for the difference between the calculated and the observed motion of the carrier.

It should be noted, too, that the motion was measured when a single shot was fired, so that there was no magazine with an incoming round bearing against the bottom of the carrier.

Since the difference between the calculated and the measured velocity of the carrier could not be attributed to friction, it appeared that the hammer was exerting a greater effect on the motion of the carrier than had been expected. Prior experiments by Werner showed that the hammer rebounded after impact on the firing pin as illustrated in Figure 37.

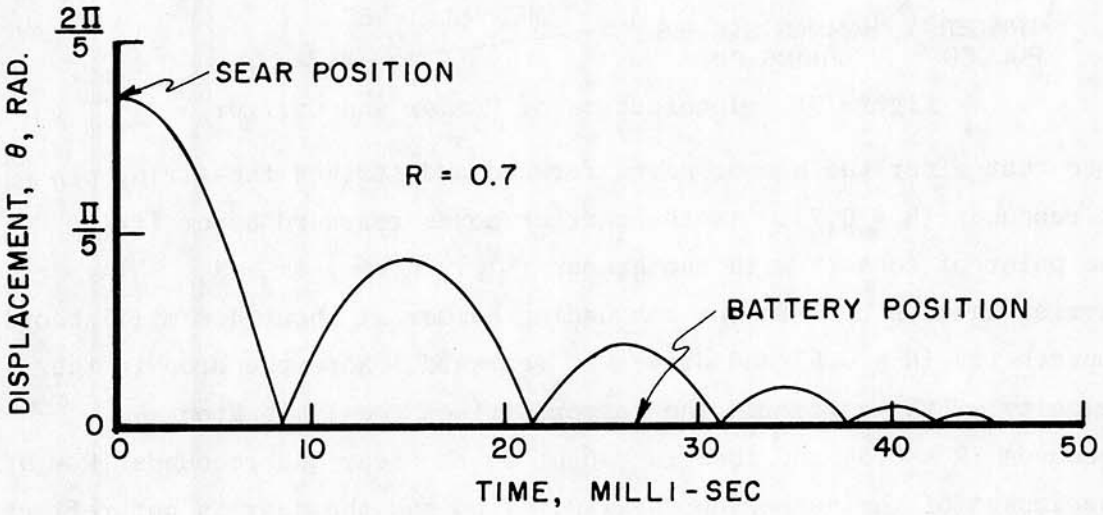

Figure 37. Hammer Rebound

The motion was measured without a round in the chamber. The rebound indicated that the coefficient of restitution was 0.7. In an actual firing the coefficient of restitution could be smaller because the firing pin deforms the copper primer cup; or it could be larger, because the primer cup (and firing pin and hammer) are sometimes driven rearward by the pressure inside the cup. In any case, a dynamic model of the hammer is required, like that described previously.

The interaction of the hammer and the carrier is shown in Figure 38.

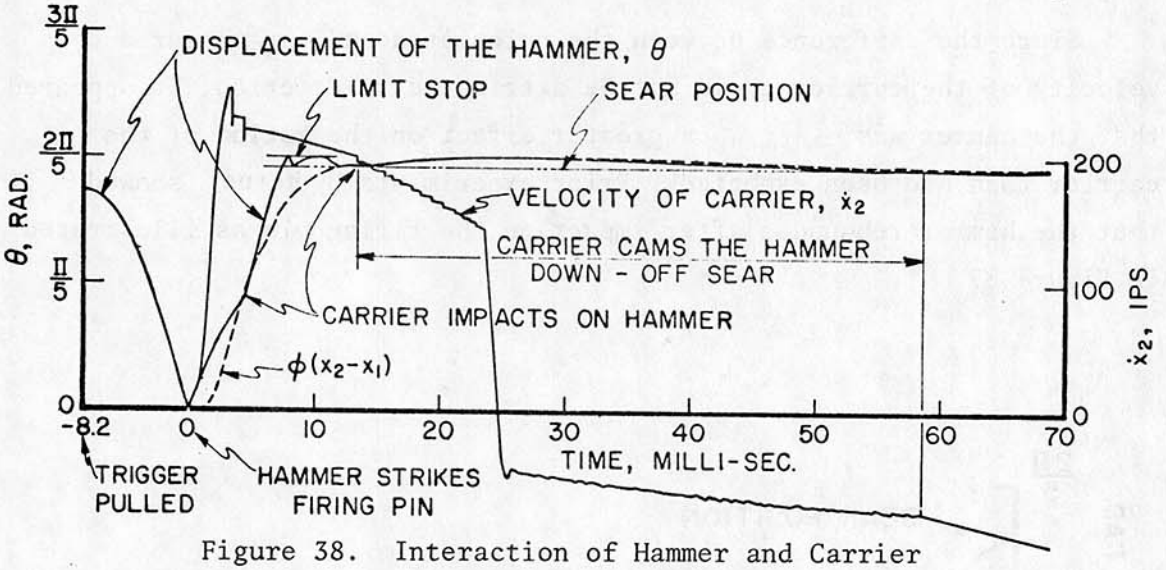

Figure 38. Interaction of Hammer and Carrier

Note that after the hammer moves forward and strikes the firing pin it rebounds (R = 0.7). As the carrier moves rearward after firing the point of contact with the hammer is given by $\phi\ (x_2 - x_1)$. The carrier catches up with the rebounding hammer at about 4.8 milliseconds, impacts it, (R = 0.5) and drives it rearward. Note the drop in the velocity of the carrier. The hammer strikes the limit stop and rebounds (R = 0.5) and then is caught on the sear and rebounds (R = 0.5). The impact of the hammer on the limit stop and the sear is not reflected in the other motion because θ is approximately 70° (see also Figure 31) and the impact forces are almost vertical. The carrier continues its rearward motion, and at about 13.5 milliseconds impacts the hammer again, camming it down off the sear. The following series of small impacts (or rubbing) has a very noticable effect on both the recoil (positive) velocity and counterrecoil velocity of the carrier. Note the change in slope of the counterrecoil velocity of the carrier as it moves forward and leaves the hammer on the sear. The polished contact surface on the bottom of the carrier is very practical evidence of the rubbing between the carrier and the hammer.

To further illustrate the importance of the hammer motion, a

phase-plane diagram of the carrier motion is shown in Figure 39. The spring force is also shown because the intersection of the spring force-distance curve with the x-axis is the center of the circle that represents the undamped motion.[13]

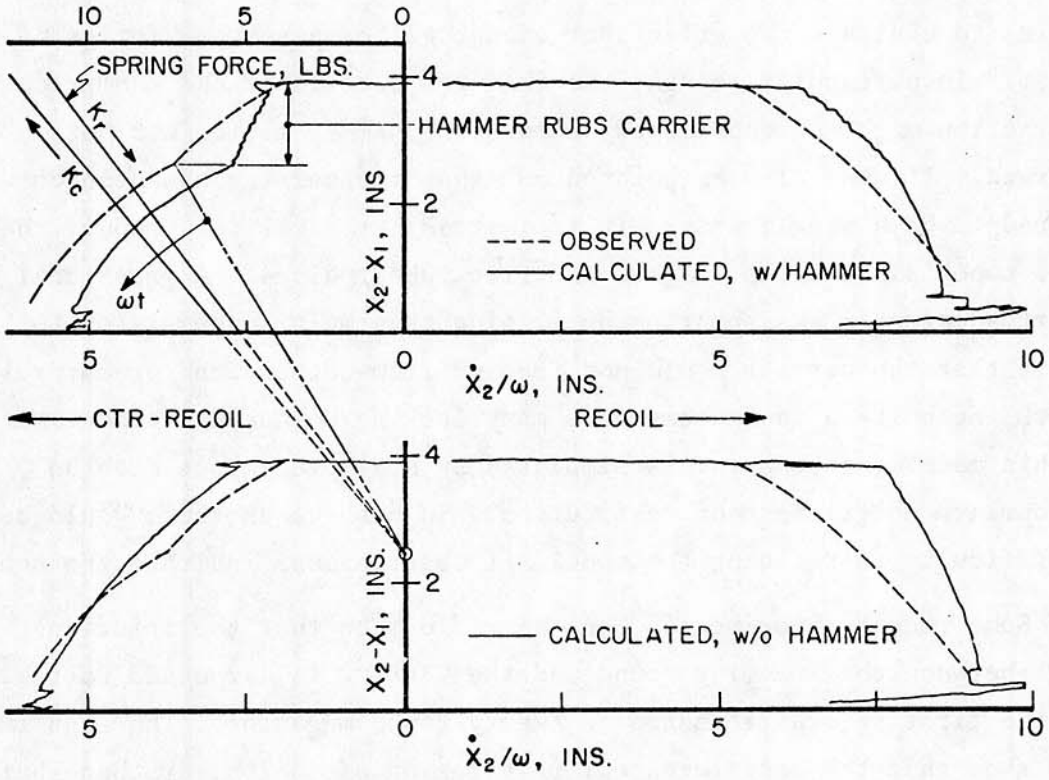

Figure 39. Phase-Plane Diagram of Carrier Motion

Note that the counterrecoil motion (top left portion) is an arc with the proper center after the carrier leaves the hammer on the sear. The calculated motion could be made to agree better with the observed motion of the carrier by adjusting the coefficients of restitution, but since the motion of the hammer was not observed, the additional refinement is not warranted. The lower part of Figure 39 shows the calculated motion of the carrier when the hammer is omitted. The observed recoil velocity is very much less, and the calculated counterrecoil velocity does not show the discontinuity.

X. RESUME

Since the output of this model of the M16 Rifle mechanism agrees reasonably well with the corresponding observations, it can be said with some certainty that the model generally should be adequate for studies to evaluate the effects of changing the masses and forces of the system. In particular though, the inferred details of the hammer-carrier interaction might be questioned because the hammer motion was not observed. It must also be pointed out that the carrier has been considered to be a single mass. It is instead: the carrier proper, the guide tube, six inertia weights and five rubber discs. A great deal of effort apparently was spent on developing this multi-mass system to insure that the carrier would not rebound from battery and prematurely unlock the bolt--a fault common to many locking-unlocking mechanisms. In this model the behavior is simulated by a simple impact with an appropriate coefficient of restitution. In both cases there would be no difficulty in refining the model, if observations indicate the need.

Some recent experiments[14] on the rifle show that the friction force between the incoming round and the carrier is large and variable for the first several rounds of a twenty-round magazine. The experiments also show that the coefficient of restitution of the polyurethane buffer button varies for the first three rounds of a burst. Neither of these effects are included in this model, but they could be added with no difficulty.

Now it may seem that a great deal of effort has been used to obtain this model, especially since the 20mm, M-139 Gun was simulated with only about half of the analog components used in this simulation. However, that simulation ignored the details of both the gas-operating system and the locking-unlocking system. As a result only two coordinate systems were used; five are used in this model of the M16 Rifle.

The need for greater, or less, detail in a model or simulation depends, of course, on the final goal, but whether or not it should be

done can be decided from the intimate relation between the engineer and the analog computer. The importance of the various parameters is established early in the process when the problem is scaled. The ability to obtain an immediate solution and the ease with which the parameters can be changed provides an immediate "sensitivity analysis" that facilitates an on-going appraisal of the adequacy of the model. In this way, the analog computer forces the engineer to understand and to refine not just the model, but also his knowledge of the actual mechanism.

This situation has provided the stimulus for some important advances in our ability to calculate the kinematics and dynamics of automatic weapons. In the very early part of this work it became obvious that a comprehensive model of the gas-operating system was required for a reasonable understanding of the dynamics of the mechanism. These models provided detailed forcing functions, and thereby brought about a need for greater detail of simultaneous resistive forces such as the cam and the unlocking forces. The aforementioned techniques for calculating the kinematics and dynamics of cam systems were therefore developed. Metal-on-metal impact is the rule rather than the exception in practically all gun mechanisms. Laird's technique for modeling such impacts had been used previously but further adaption and more concise definition of the damping parameters in the two-body problem had to be devised for this study. More importantly, the technique was extended to describe the combination of linear and angular impact, which was required to model the carrier-hammer interaction.

As a consequence, the most important aspect of this report is that the techniques developed for simulating the forces acting on the M16 Rifle mechanism provide the engineer with the basic tools for modeling other self-powered automatic weapon mechanisms.

ACKNOWLEDGMENTS

Mr. W. M. Werner should be considered a coauthor of this report because he was originally assigned this task and completed the physical measurements, firing tests, and some of the analog computer work prior to his resignation.

The authors are indebted to Mr. T. Brosseau for carrying out some confirmatory measurements of spring and friction forces.

REFERENCES

1. "Operational Reliability Test of the M-16A1 Rifle System" (FOUO), WSEG Report, Feb 1968.

2. Robert W. Geene, "Computer Simulation of 5.56mm Propellants," Ballistic Research Laboratories Memorandum Report No. 1937, Sep 1968, AD842807.

3. Joseph H. Spurk, "The Gas Flow in Gas-Operated Weapons," Ballistic Research Laboratories Report No. 1475, Feb 1970, AD704342.

4. Nathan Gerber, "Sensitivity Study of Rifle Gas Systems, "Ballistic Research Laboratories Report No. 1524, Jan 1971, AD880431.

5. W. M. Werner, "Comparison of a Theoretical and Experimental Study of the Gas System in the M16A1 Rifle," Ballistic Research Laboratories Report No. 1548, Aug 1971, AD731218.

6. Herman P. Gay and Emma M. Wineholt, "Analog Simulation of Ring Spring Recoil Systems," Ballistic Research Laboratories Memorandum Report No. 1826, Mar 1967, AD651309.

7. Herman P. Gay and Emma M. Wineholt, "Analog Simulation of the 20MM Gun, M139," Ballistic Research Laboratories Report No. 1436, Jun 1969, AD855145.

8. "Rifle, 5.56-MM, M16; Rifle, 5.56-MM, XM16E1; and Launcher, Grenade, 40-MM, XM148," TM 9-1005-249-14, 1 August 1966.

9. J. P. Laird, J. R. Ashley, and W. A. Kelly, "That's the Way the Ball Bounces... or is it?," Simulation: Technical Journal of Simulation Councils, Inc., Vol. 4, No. 5, May 1965, pp. 294-305.

10. J. Corner, Theory of the Interior Ballistics of Guns, New York, John Wiley and Sons, Inc., 1950, p. 327.

11. Emma M. Wineholt, "Analog Circuits for Reproducing a Measured Pressure-Time Curve in a Gun," Ballistic Research Laboratories Technical Note No. 1737, June 1970, AD873105.

12. Herman P. Gay, "The Dynamics of Cam Systems for Gun Mechanisms," Ballistic Research Laboratories Memorandum Report No. 2177, Mar 1972, AD741360.

13. H. P. Gay, "On Calculating the Motion of Recoil Systems for Automatic Weapons by the Phase Plane Method," Ballistic Research Laboratories Report No. 874, June 1953, AD23469.

14. Timothy L. Brosseau, "Kinematic Study of the M16A1 Rifle," Ballistic Research Laboratories Memorandum Report No. 2153, Jan 1972, AD892463L.

DISTRIBUTION LIST

No of Copies	Organization
2	Commander Defense Documentation Center ATTN: TIPCR Cameron Station Alexandria, VA. 22314
1	Director Weapons System Evaluation Group Dept. of Defense Washington, D. C. 20305
1	Commanding General U.S. Army Materiel Command ATTN: AMCDL Washington, DC 20315
1	Commanding General U.S. Army Materiel Command ATTN: AMCRD, Dr. J.V.R. Kaufman Washington, DC 20315
1	Commanding General U.S. Army Materiel Command ATTN: AMCRD-TE Washington, DC 20315
1	Commanding General U.S. Army Materiel Command ATTN: AMCRD-TP Washington, DC 20315
1	Commanding General U.S. Army Aviation Systems Command ATTN: AMSAV-E 12th & Spruce Streets St. Louis, Missouri 63166
1	Commanding General U.S. Army Electronics Command ATTN: AMSEL-DL Fort Monmouth, New Jersey 07703
1	Commanding General U.S. Army Missile Command ATTN: AMSMI-R Redstone Arsenal, AL 35809
2	Commanding General U.S. Army Tank-Automotive Command ATTN: AMSTA-RHFL AMSTA-CL, Dr. Petrick Warren, Michigan 38090
2	Commanding Officer U.S. Army Mobility Equipment Research & Development Center ATTN: Tech Docu Cen, Bldg. 315 AMSME-RZT Fort Belvoir, VA 22060
1	Commanding General U.S. Army Munitions Command ATTN: AMSMU-RE Dover, New Jersey 07801
1	Director U.S. Army MUCOM Operations Research Group Edgewood Arsenal, Md 21010
6	Commanding Officer U.S. Army Frankford Arsenal ATTN: Dr. S. Ross SMUFA-Lib SMUFA-J7700, Mr. F. Shinaly SMUFA-J8000, Mr. J. Mitchell SMUFA-J9000, Mr. W. Davis SMUFA-J1100, Mr. H. Rosenberg Philadelphia, Pennsylvania 19137

DISTRIBUTION LIST

No of Copies	Organization
2	Commanding Officer U.S. Army Picatinny Arsenal ATTN: SMUPA Mr. W. Painter SMUPA-VC2, Mr. G. Demitrack Dover, New Jersey 07801
3	Commanding General U.S. Army Weapons Command ATTN: AMSWE-SIH Rock Island, Illinois 61202
3	Commanding General U.S. Army Weapons Command ATTN: AMSWE-RE AMSWE-RDF AMSWE-RES Rock Island, Illinois 61202
4	Commanding General U.S. Army Weapons Command ATTN: AMSWE-REA AMSWE-RET AMCDM-R AMCPM-VRF Rock Island, Illinois 61202
3	Commanding Officer U.S. Army Watervliet Arsenal ATTN: SWEWV-RD, Dr. Weigle SWEWV-RDD, Mr. V. Preska Mr. F. John Watervliet, New York 12189
1	Director U.S. Army Advanced Materiel Concepts Agency 2461 Eisenhower Avenue Alexandria, Virginia 22314
1	Director U.S. Army Air Mobility Research & Development Laboratory Ames Research Center Moffett Field, Calif. 94035
1	Commanding Officer U.S. Army Harry Diamond Laboratories ATTN: AMXDO-TD/002 Washington, DC 20438
2	Commanding Officer U.S. Army Materials & Mechanics Research Center ATTN: AMXMR-ATL AMSMR-T Mr. F. Baratta Watertown, Massachusetts 02172
1	Commanding General U.S. Army Natick Laboratories ATTN: AMXRD-Dr. D. Sieling Natick, Massachusetts 01762
1	CDC Systems Analysis Group Ft. Belvoir, VA 22060
1	HQ DA (DACS-CW) Washington, DC 20310
1	HQ DA (DARD-ARP) Washington, DC 20310
1	Commanding Officer U.S. Army Research Office (Durham) ATTN: Dr. Kumar Box CM Duke Station Durham, North Carolina 27706
1	Department of Ordnance U.S. Military Academy ATTN: Assoc Prof West Point, New York 10996
1	University of Michigan Department of Mechanical Engineering ATTN: Prof J. Shigley Ann Arbor, Michigan 48104

DISTRIBUTION LIST

No of Copies	Organization
3	Commander U.S. Naval Air Systems Command ATTN: AIR-604 Washington, DC 20360
3	Commander U.S. Naval Ordnance Systems ATTN: ORD-0632 ORD-035 ORD-5524 Washington, DC 20360
2	Commander U.S. Naval Weapons Center ATTN: Code 753 Code 12 China Lake, Calif. 93555
1	Commanding General Marine Corps Development & Education Center ATTN: Chief, Ground Oprs Div. Development Center Quantico, VA 22134

Aberdeen Proving Ground

Chief, Tech Lib
Marine Corps Ln Ofc
CDC Ln Ofc
CO, USASASA
ATTN: Mr. Ambrosine
(10 cys)
Dir, MTD
ATTN: Small Arms Br.
(3 cys)
Dir, AMSAA
ATTN: Mr. Simmons
Mr. Clifford
Dr. Sperrazza
Mr. Kramer
Mr. M. Smith
Dir, HEL
ATTN: Mr. Torre

Unclassified

Security Classification

DOCUMENT CONTROL DATA - R & D

(Security classification of title, body of abstract and indexing annotation must be entered when the overall report is classified)

1. ORIGINATING ACTIVITY *(Corporate author)*

U.S. Army Aberdeen Research and Development Center
Ballistic Research Laboratories
Aberdeen Proving Ground, Maryland

2a. REPORT SECURITY CLASSIFICATION

Unclassified

2b. GROUP

3. REPORT TITLE

Analog Simulation of the Mechanism of the M16A1 Rifle

4. DESCRIPTIVE NOTES *(Type of report and inclusive dates)*

5. AUTHOR(S) *(First name, middle initial, last name)*

Herman P. Gay, Emma M. Wineholt

6. REPORT DATE	7a. TOTAL NO. OF PAGES	7b. NO. OF REFS
June 1972	59	14

8a. CONTRACT OR GRANT NO. This work was sponsored by Project Manager, Rifles

~~b. PROJECT NO.~~ under AMCMS Code No. 4420.16.0132.251

and PRON No. 45-9-76500-(02)-45-AJ

9a. ORIGINATOR'S REPORT NUMBER(S)

Report No. 1596

9b. OTHER REPORT NO(S) *(Any other numbers that may be assigned this report)*

10. DISTRIBUTION STATEMENT

Distribution limited to U.S. Government agencies only. Other requests for this document must be referred to Director, U.S. Army Ballistic Research Laboratories, ATTN: AMXBR-XSE, Aberdeen Proving Ground, Maryland 21005

11. SUPPLEMENTARY NOTES

12. SPONSORING MILITARY ACTIVITY

U.S. Army Materiel Command
Washington, D.C.

13. ABSTRACT

The mechanism of the M16 Rifle has been simulated in some detail on the analog computer. This simulation yields the linear motion of the gun, the linear and the angular motion of the bolt, the linear motion of the carrier and the angular motion of the hammer. During the course of the work techniques were adapted and extended for calculating linear impulsive motion, a combination of linear and angular impulsive motions and the dynamics of cam systems. As a result, the output of the simulation agrees rather well with the measured motion. However, the more important aspect of this study is that the engineer now has at hand the basic techniques, or tools, for modeling self-powered automatic weapon mechanisms.

DD FORM 1 NOV 68 1473 REPLACES DD FORM 1473, 1 JAN 64, WHICH IS OBSOLETE FOR ARMY USE.

Unclassified

Security Classification

14. KEY WORDS	LINK A		LINK B		LINK C	
	ROLE	WT	ROLE	WT	ROLE	WT
dynamics						
kinematics						
automatic weapons						
mechanisms						
analog						
simulation						
cams						
impulsive motion						